Review

Current Developments in the Effective Removal of Environmental Pollutants through Photocatalytic Degradation Using Nanomaterials

Chandhinipriya Sivaraman [1], Shankar Vijayalakshmi [2], Estelle Leonard [3], Suresh Sagadevan [4,*] and Ranjitha Jambulingam [2,*]

[1] School of Advanced Sciences, Vellore Institute of Technology, Vellore 632014, India; schandhinipriya@gmail.com
[2] CO2 Research and Green Technologies Centre, Vellore Institute of Technology, Vellore 632014, India; vijimicro21@gmail.com
[3] Laboratoire TIMR UTC-ESCOM, Centre de Recherche de Royallieu, Rue du Docteur Schweitzer, CS 60319, CEDEX, F-60203 Compiègne, France; e.leonard@escom.fr
[4] Nanotechnology & Catalysis Research Centre, University of Malaya, Kuala Lumpur 50603, Malaysia
* Correspondence: drsureshsagadevan@um.edu.my (S.S.); jranji16@gmail.com (R.J.)

Abstract: Photocatalysis plays a prominent role in the protection of the environment from recalcitrant pollutants by reducing hazardous wastes. Among the different methods of choice, photocatalysis mediated through nanomaterials is the most widely used and economical method for removing pollutants from wastewater. Recently, worldwide researchers focused their research on eco-friendly and sustainable environmental aspects. Wastewater contamination is one of the major threats coming from industrial processes, compared to other environmental issues. Much research is concerned with the advanced development of technology for treating wastewater discharged from various industries. Water treatment using photocatalysis is prominent because of its degradation capacity to convert pollutants into non-toxic biodegradable products. Photocatalysts are cheap, and are now emerging slowly in the research field. This review paper elaborates in detail on the metal oxides used as a nano photocatalysts in the various type of pollutant degradation. The progress of research into metal oxide nanoparticles, and their application as photocatalysts in organic pollutant degradation, were highlighted. As a final consideration, the challenges and future perspectives of photocatalysts were analyzed. The application of nano-based materials can be a new horizon in the use of photocatalysts in the near future for organic pollutant degradation.
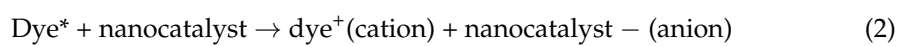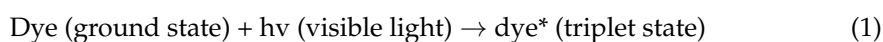
1. Introduction

Massive advancements in nanoscience and technology mean they emerged as promising solutions for environmental clean-up and the production of energy in recent decades. Nanomaterials (NMs) have opened up many new possibilities for a variety of manufacturing/industrial applications over the years, including wastewater treatment and the removal of hazardous contaminants from the atmosphere. The advancement in industrialization leads to the release of toxins, with the emission of hazardous chemicals into the atmosphere. In this regard, methods such as immobilization, biological and chemical oxidation, and incineration were widely used to treat a variety of organic and toxic industrial contaminants. Nanomaterials have the peculiarity of changing the characteristics of materials through their optical, magnetic, and electrical properties, and are helpful in many processes and applications [1]. Nanomaterials are used in many fields, from electricity to medicine, because of their unique physicochemical and biological properties [2]. Recently, visible light-induced heterogeneous photocatalysis developed rapidly,

due to its advantage in the implementation of environmental remediation, particularly in wastewater treatment [3]. Nowadays, anthropogenic chemicals used in agriculture, medicine, the military, and industry directly enter the water stream easily, which causes an adverse effect on the environment, and risks the contamination of both surface and groundwater [4]. As a result of this water contamination, endocrine disruptors interfere with the normal hormonal system, which causes adverse health effects such as birth defects and developmental disorders in children, infertility, and cancerous tumors, and also causes several water-borne diseases. According to the World Health Organization, half of the world's population will suffer due to the water crisis by 2025. Environmental pollution is one of the most consequential issues currently faced all over the world and could be resolved by creating the conditions to achieve a clean and healthy environment for a better life in the world. In recent decades, population and global production growth resulted in much higher production of chemicals, due to their daily entry into the environment and resistance to biodegradation, resulting in the generation of hazards for various species. To prevent water and environmental pollution caused by the arrival of polluted industrial effluents, appropriate strategies for their treatment and reuse must be developed. Today, safe and hygienic drinking water is a unique requirement of the global health community. The clustering of densely populated and industrial areas close to water resources magnified global issues. The new approach, e.g., via an oxidative pathway, makes a distinguishing change in the removal of environmental pollutants. Photocatalysis is applicable at room temperature and pressure consumes less energy and profits from process simplicity. Several technologies are available in the wastewater treatment process, such as electrodialysis [5], membrane filtration [6], precipitation adsorption [7], electrochemical reduction [8], and electrodeionization [9]. They are very expensive and complicated, and by transferring pollutants between fluids, various wastes and by-products are generated that make it difficult to treat wastewater. Recently, photocatalysis became a viable technology for the treatment of various pollutants present in wastewater [10].

Photocatalytic reactors may play an increasingly important role in new technologies for the filtration of organic-polluted water [11–13]. The degradation of different organic contaminants with better competence utilizes heterogeneous photocatalyst-based nanoparticles. Photocatalysis gained a lot of interest in recent years, because of green energy and environmental cleanup. As a result, there are numerous reviews on the subject, focused on various types of photocatalysts and photocatalyst applications. Furthermore, there were few basic developments in the concept, and no notable breakthroughs were observed in photocatalyst plans in the past five years. There is still much work to do, both in terms of making these materials practical (which is debatable for some applications), and in terms of improving our understanding of the complex processes, particularly in some of the more complicated ternary or quaternary photocatalysts proposed. Since key works by Honda and Fujishima in 1972, and Reiche and Bard in 1979 [14,15], there was a surge in interest in photocatalysis. Many other photocatalyst materials and uses were studied, but commercial photocatalysis applications were uncommon. Low photocatalytic activity, particularly under visible or solar illumination, is usually blamed for the lack of commercial uses. As a result, significant resources were invested in the development of improved photocatalyst materials. Material development techniques for different types of photocatalysts were focused on maximizing efficiency by targeting one or more phases in the photocatalytic reaction. Several studies reported on the treatment of wastewater using different photocatalysts. The photocatalytic degradation of pollutants is mainly focused on the formation of highly reactive hydroxyl radical ions. These photocatalytic reactions are triggered by the free radical mechanism initiated by the interaction of photons using the catalysts. Therefore, in the present review paper, we mainly focused on the recent advances in photocatalytic pollutant removal from wastewater, and also elaborated in detail on the factors affecting the performance of the photocatalytic degradation of pollutants to remove them from wastewater.

2. Photocatalytic Degradation Mechanism of Dyes

A photocatalytic reaction is primarily determined by the wavelength of light (photon) energy and the catalyst. Nanomaterials used as catalysts, such as NiO, TiO_2, ZnO, ZnS, and others, are referred to as nanocatalysts. The light can be irradiated directly or indirectly, as a result of the catalyst reacting with the dye. The photocatalytic mechanism associates dye degradation with the redox capabilities, or potential, of dyes and the energy level of the conduction band of the semiconductor, or nanomaterial, used. Photocatalysis degrades dyes via photosensitization, i.e., direct, or self, dye degradation and photo-oxidation by a reactive species (catalyst), or indirect dye degradation. Both photocatalytic mechanisms rely on electronic structures, specifically the band structure of the catalyst and the dye. Due to their electronic structure, which is described by a filled valence band and an empty conduction band, nanocatalysts act as chemical activators for the illumination of light-animated redox processes. The photosensitization mechanism, also known as the direct mechanism of dye degradation, absorbs visible light. The dye is excited from the ground state to the triplet excited state, using visible light photons with wavelengths greater than 400 nm. An electron addition into the conduction band of nanocatalysts, transferred from the valence band, converts this excited state of the original dye species into a semi-oxidized radical cation (Dye^+). The reaction between these trapped e-/h+ pairs and the dissolved oxygen in the system results in the formation of superoxide radical anions (O_2^-), and the formation of hydroxyl radicals (OH). In nature, this hydroxyl radical is non-reactive, and is primarily responsible for the oxidation of the organic compounds represented by Equations (1) and (2) below:

$$\text{Dye (ground state)} + hv \text{ (visible light)} \rightarrow \text{dye* (triplet state)} \tag{1}$$

$$\text{Dye*} + \text{nanocatalyst} \rightarrow \text{dye}^+\text{(cation)} + \text{nanocatalyst} - \text{(anion)} \tag{2}$$

According to several researchers, visible light acts as a driving source in photosensitization, which occurs at a very slow rate. In contrast, an indirect mechanism, known as photo-oxidation/photocatalysis, in which a catalyst sensitizes the chemical reaction for dye degradation, is found to be more prevalent than a direct mechanism. The mechanism of dye degradation is based primarily on oxidation and the reduction of the photocatalyst, as shown in Figure 1. When photons of light strike a material, they excite electrons from the valence band to the conduction band, which results in the development of electron-hole pairs. The electrons in the conduction band react with the oxygen molecule to form superoxide radical anions; however, the holes in the valence band react with effluent water to form hydroxyl radicals.

Basic Principles of Z-Scheme Photocatalysis

In photocatalysis, the Z-scheme represents/mimics the natural photosynthesis system, which has advantages such as charge separation and delayed recombination, which increases the light harvest and improves redox ability [16], as shown in Figure 2. The light absorption and production of photogenerated electron-hole pairs are the first steps. The carriers of photogenerated electrons then move to the surface, where they recombine or participate in surface redox processes. By ensuring effective charge separation, and increasing surface redox reactions, photocatalytic performance improves to maximize light absorption, maximize charge transfer at the surface, and minimize recombination. Common techniques investigated for performance improvement include morphology optimization (which can affect the surface active sites as well as charge separation), doping (which can reduce the bandgap, and sometimes has negative effects on recombination losses), using sensitizers and/or co-catalysts (to increase visible absorption, as well as provide more active sites and affect carrier dynamics), and using different materials. Photocatalytic reactors can play an efficient role in novel technologies for the purification of water polluted with organic chemicals [13]. The degradation of various organic pollutants, using nanoparticle-based heterogeneous photocatalysts with higher efficiency, is reported, and shown in Table 1.
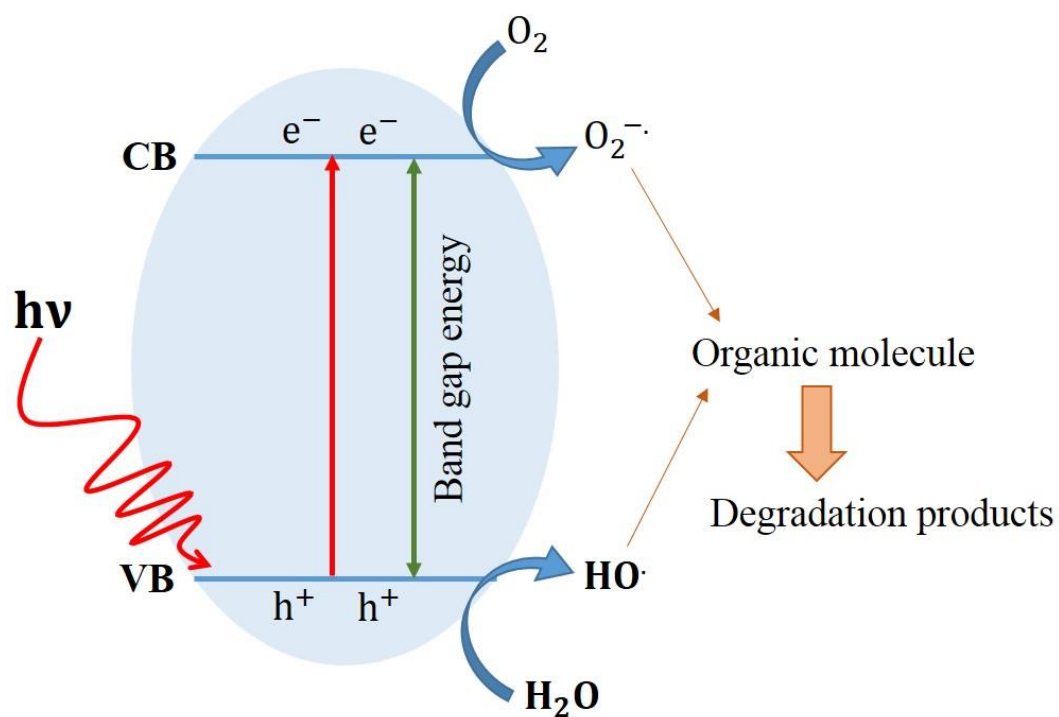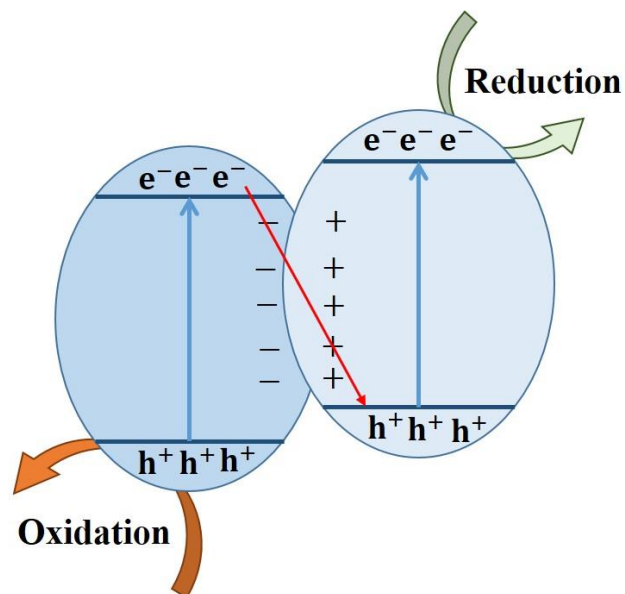
Figure 1. Schematic diagram of photocatalytic process.

Figure 2. Schematic diagram of Z-scheme in photocatalysis.

Table 1. Degradation of organic pollutants using photocatalyst-based nanomaterial.

Materials	Pollutant	Degradation Efficiency	References
CuO nanosheets	Allura Red AC	~96.99% in 6 min	[17]
MFe$_2$O$_4$: (M = Co, Ni, Cu, Zn)	Methyl red Methyl orange Methylene blue Bromo green	78% in 50 min 92% in 50 min 89% in 50 min 93% in 50 min	[18]
α-Bi$_4$V$_2$O$_{11}$	Rhodamine B	100% in 45 min	[19]
m3D–TiO$_2$–HP Graphene	Hexavalent Chromium	96% in 70 min	[20]
TiO$_2$–graphene	Acid Black 1 dye	96% in 40 min	[21]
TiO$_2$–graphite composite	Paracetamol	100% in 120 min	[22]
Mg–ZnO–Al$_2$O$_3$	Caffeine	98.9% after 70 min	[23]
Zr/Ag–ZnO	Acid Black 1 dye	99.3% after 40 min	[24]
CeO$_2$	Yellow 6G dye	100% within 30 min	[25]
Al$_2$O$_3$–NP/SnO$_2$	Methyl orange	93.95% in 50 min	[26]
TiO$_2$ Degussa P25	Rhodamine B	33% in 180 min	[27]
CuO–GO/TiO$_2$	2-Chlorophenol	86% in 210 min	[28]
Copper nanoparticles	Methylene blue	91.53% in 30 min	[29]
Copper nanoparticles	Congo red	84.89% in 30 min	
CuO nanorods	Reactive Black Dye	98% in 300 min	[30]
Cu/Cu (OH)$_2$	Rhodamine B	99.99% in 120 min	[31]
CuO–Cu$_2$O/GO	Tetracycline	90% after 120 min	[32]
Copper nanoparticles	Phenyl red	99.62% in 15 min	[33]
Cds/CuS	Methyl orange	93% in 150 min	[34]
Bismuth-doped copper aluminate	Methylene blue	99.9% in 60 min	[35]

3. Removal of Polybrominated Diphenyl Ethers (PBDEs)

Polybrominated diphenyl ethers (PBDEs) are the second most commonly used BFRs, and their molecular structure is similar to polychlorinated biphenyls (PCBs). In general, these BDEs are available commercially as mixtures in three different forms, namely, penta-, octa-, and deca-mixes. Penta-BDE is used in polyurethane foams and textiles; octa-BDE is used in styrenes, polycarbonates, and thermosets; and deca-BDE is used in synthetic textiles and electronics. As a successful replacement for PCBs, these PBDEs are found in all levels of ecosystems, and are able to redistribute globally among these ecosystems. They pose a threat to the human population, indigenous peoples, and fish consumers, as they bio-accumulate in the food chain and are highly lipophilic, similar to dioxins and PCBs [36]. Unfortunately, this accumulation of PBDEs affects motor skills and disturbs the metabolism of the thyroid hormone; hence, it is classified as a high-risk pollutant that causes serious environmental pollution. Dietary intake and dust ingestion are the dominant human exposure pathways. PBDEs were widely detected in human samples, especially in human serum and human milk. Data shows that PBDEs are generally declining in human samples worldwide, as a result of their phasing out. Due to the common use of PBDEs, their levels in humans from the USA are generally higher than that in other countries. High concentrations of PBDEs were detected in humans from PBDE production regions and e-waste recycling sites. BDE-47, -153, and -99 were proven to be the primary congeners in humans. Human toxicity

data demonstrates that PBDEs have extensive endocrine disruption effects, developmental effects, and carcinogenic effects among different populations, as shown in Figure 3. Besides bio-accumulation, exposure to this toxic chemical during its production, processing, and recycling causes adverse effects in human beings. In fact, air and dust are proven to show measurable PBDE concentrations, and inhaling it could account for up to one-quarter of total exposure. Generally, several remediation techniques are followed for remediating this harmful chemical; and these include hydrothermal, adsorption, photolysis, advanced oxidative processes, and photocatalytic degradation, etc. Specifically, photocatalysis and photocatalytic degradation are regarded as the most common and reported methods for remediating these PBDEs. The most commonly studied PBDEs include their congeners BDE-47 and BDE-209, owing to both their toxicity and their intermediate products. To begin with, Azri et al. (2016) [37] use a tri-metallic catalyst, $Cu/Ni/TiO_2/PVC$, prepared using sol-gel and a hydrothermal method, and report the rate of degradation of PBDE as 65.82% [37]. Likewise, Wang et al. (2019) [38] use a metal-doped TiO_2 photocatalyst for degrading dibrominated diphenyl ethers under photocatalytic degradation; while, Li et al. (2014) [39] carry out the photocatalytic debromination of PBDEs using a Pd/TiO_2 catalyst, and conclude that TiO_2 enhances the rate of debromination upon increasing the loading of palladium. Similarly, Lei et al. (2016) [40] prepare debrominated PBDEs using $Ag–TiO_2$ under the influence of UV light, and note that the debromination is rapid. This study concludes that the effectiveness of debromination PBDEs using metal-doped TiO_2 is enhanced based on the metal additive; but reduces drastically upon using metal-doped TiO_2 catalysts exposed to air [39,40]. In addition, replacing Pd with Cu enhances the rate of electron transfer from the conduction band of TiO_2 to PBDEs [41]. It is worth mentioning that the degradation of PBDE is carried out in two different processes, with electrons sourced from striking photons favoring reduction debromination; holes or •OH generated as a result of photocatalytic reaction favor oxidation debromination. Moreover, the redox photoreduction of PBDEs using nanomaterial-based catalysts is adversely affected by the recombination of holes and electrons. However, adding water and irradiation using UV light simply enhances the rate of oxidative degradation of PBDEs, especially BDE-209 [42]. The degradation of various polybrominated diphenyl ethers, using nanoparticle-based heterogeneous photocatalysts with higher efficiency, is reported and shown in Table 2.
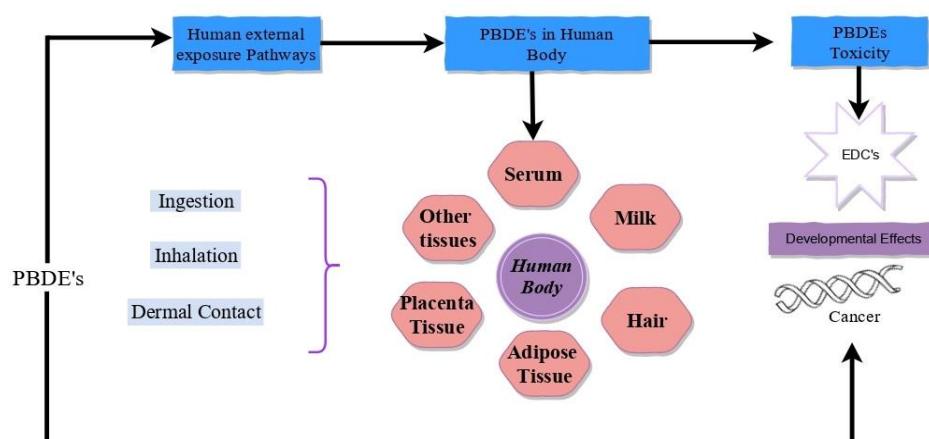

Figure 3. Human exposure to PBDEs and their health outcomes.

Table 2. Degradation of various polybrominated diphenyl ethers using nanoparticle-based heterogeneous photocatalysts.

Pollutant	Photocatalyst	Light	Results	References
BDE-209	TiO_2	UV lamp	Debromination efficiency of BDE-209 achieved, up to 95.6%	[43]
BDE-209	RGO/TiO_2	UV lamp	Debromination efficiency of BDE-209 achieved, up to 59.4%	[44]
BDE-47	RGO/TiO_2	Xe lamp	Debromination efficiency of BDE-47 achieved, up to 25%	[45]
BDE-209	CuO/TiO_2	Xe lamp	Debromination of ten PBDEs was achieved under anaerobic conditions	[46]
BDE-209	FeOCN-x	Visible Xe lamp	Higher photocatalytic activity for debromination of PBDEs was achieved	[47]
BDE-209	$AgI–TiO_2$	Xe lamp	The addition of silver iodide to the surface of TiO_2 increased the debromination efficiency of BDE-209	[48]
BDE-47	$Ag@Ag_3PO4/g-C_3N_4/rGO$	UV lamp	Debromination efficiency of BDE-47 was achieved, up to 93.4%	[49]
BDE-47	Nickel nanoparticles	Visible lamp	Debromination of BDE-47 was achieved completely under visible irradiation	[50]
BDE-47	Ag/TiO_2	UV lamp	Ag/TiO_2 addition accelerates BDE-47 photodegradation efficiency	[51]

4. Removal of Phthalates and Their Derivative

Phthalates, or phthalate esters (PAEs), are di-esters of phthalic acid (1,2-benzene dicarboxylic acid) and are used as plasticizers for polymers to reduce their glass transition temperature, in order to induce softness and workability. In terms of classification, low-molecular-weight phthalates (dimethyl phthalate (DMP), diethyl phthalate (DEP), and dibutyl phthalate (DBP)) are used in small to medium scale commercial applications (plastic containers, materials packaging, personal care products, solvents, adhesives, lubricants, coatings, and varnishes); high-molecular-weight phthalates (such as di-n-octyl phthalate (DOP) and di-(2-ethylhexyl) phthalate (DEHP)) are used in construction and furniture industries, as shown in Figure 4. Interestingly, these phthalates are chemically bonded during polymer manufacturing, and remain inert in leaching out into the environment; they create physical bonds upon being used as plasticizers, thereby causing them to leak into the environment. As a result, these phthalates are found all around the globe and are treated as harmful environmental pollutants, as they disrupt the endocrine glands, causing severe disturbances in the functioning of hormones inside the human body, in addition to causing genetic and reproductive abnormalities in different living organisms [52–54]. The

aforementioned phthalate compounds are deemed as high-risk pollutants and are cited as the predominant source of phthalate exposure, via inhalation, dermal contacts, and consuming contaminated foods.
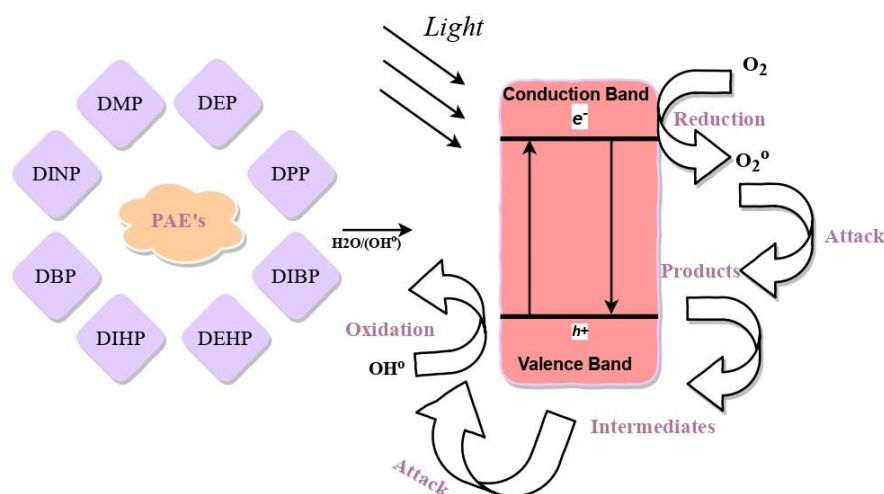

Figure 4. Photocatalytic degradation of phthalate-based compounds.

Numerous methods were suggested by different researchers, with the aim of remediating this toxic organic chemical; however, photocatalytic degradation is considered the optimum, as the catalysts provide alternative charge transfer pathways, instead of electron-hole pair recombination, and increase the surface area for adsorption. Supporting this, Kaur et al. (2019) [55] study the photocatalytic degradation of DEP using transition-metal-doped (Ni, Mn, and Co) TiO_2 nanoparticles based on their degradation rate; they recommend Mn-doped TiO_2 as an ideal catalyst, as it requires minimal excitation energy (visible light activation), owing to the lowest optical band gap being 2.47 eV. Moreover, this study concludes that doped TiO_2 catalysts perform well when compared to their undoped counterparts [55]. Likewise, Akbari-Adergani et al. (2018) [56] suggest another set of transition metals (Fe, Ag, and Co), doped in ZnO, as an effective photocatalyst for remediating DBP; they perform well (90% degradation) under visible LEDs as a light source. Similarly, Motlagh et al. (2020) [57] fabricate ZnFe-layered double hydroxides, using sulfate-intercalated anion (ZnFe-SO4−LDH) modified with graphene oxide (GO) as a photocatalyst for degrading phenazopyridine hydrochloride (PhP) under visible light irradiation; they report a maximum rate of degradation as 60.01% [57]. In addition to immobilizing photocatalysts, nanocomposites with magnetic nanoparticles, such as zero-valent iron (ZVI) were developed, which simplified the post-degradation separation simply by using magnetic properties [58,59]. Another method suggests the removal of TiO_2 from the reaction solution by an electrocoagulation technique using iron electrodes and reports 95% of TiO_2 removal under a neutral pH and 100 mA current supply. Here, the electrochemical sludge is taken as a catalyst for activating peroxymonosulfate (PMS) in order to degrade emerging contaminants because of the presence of iron species (i.e., Fe_3O_4) [60]. The degradation of various phthalates and their derivatives, using nanoparticle-based heterogeneous photocatalysts with higher efficiency, is reported and shown in Table 3.

Table 3. Degradation of various phthalates and their derivatives using nanoparticle-based heterogeneous photocatalysts.

Phthalates	Photocatalyst	Light Source	Key Results	References
DMP	Bifunctional TiO2 {001}	UV light	Nearly 76% of DMP is degraded within 120 min	[61]

Table 3. *Cont.*

Phthalates	Photocatalyst	Light Source	Key Results	References
DEP	Bifunctional TiO_2 {001}	UV light	Nearly 85% of DEP is degraded within 120 min	[61]
DEP	TiO_2 (anatase)	Xenon lamp	Photocatalytic degradation of DEP was achieved up to 90% within 50 min	[62]
DEP	Zinc oxide	Hg lamp	Photocatalytic degradation of DEP was achieved up to 80% within 30 min	[63]
DMP	Hydrothermal (h-t) and TiO_2	UV lamp	DMP removal under h-t TiO_2 (62.1%) s–g TiO_2 (33.6%)	[64]
DBP	TiO_2 (P25)	Xe lamp	DBP removal from wastewater was achieved up to 90% within 30 min	[65]
DBP	α-Fe_2O_3 nanoparticles	Mercury lamp	Photocatalytic degradation of DBP was achieved up to 90% within 120 min	[66]
BBP	P25 TiO_2	UV lamp	Photocatalytic degradation of BBP was achieved up to 80% within 60 min	[67]
BBP	Cl-doped TiO_2	Xe lamp	Up to 92% of BBP was degraded within 240 min	[68]
BBP	P-doped TiO_2 thin-films	Xe lamp	98% of BBP degradation efficiency was achieved within 180 min	[69]
DEHP	N_x–TiO_{2-x}	Xenon	When compared to TiO_2 Degussa P25, N-doped TiO_2 shows a faster rate of DEHP degradation up to 90%	[70]
DEHP	Fe-Ag/ZnO	Visible lamp	About 90% of DEHP was removed within 150 min	[71]
DMP	N-doped TiO_2 (UN/TiO_2)	Visible light	DMP is removed at a degradation rate of 41% and 58% using N/TiO_2 and UN/TiO_2 within 5 h	[72]
DEP	Ni/TiO_2; Mn/TiO_2; Co/TiO_2	Hg lamp	DEP was degraded up to 92% within 1hr 30 min	[73]

Table 3. *Cont.*

Phthalates	Photocatalyst	Light Source	Key Results	References
DEP	WO_3/TiO_2	UV light	The photodegradation of DEP under visible light is achieved, up to 90% within 60 min	[74]
DBP	Bi, Cu co-doped $SrTiO_3$	Metal halide lamp	Nanosized Bi, Cu co-doped $SrTiO_3$ showed significant degradation efficiency than bi-doped $SrTiO_3$	[75]
DBP	m-TiO_2-NTs (mesoporous TiO_2 nanotubes)	Mercury lamp	DBP removal degradation rate constant for m-TiO_2-NTs; 7.7 times greater than that of TiO_2	[76]
DBP	Carboxymethylβ-cyclodextrin Fe_3O_4_TiO_2	Mercury lamp	In comparison to Fe_3O_4–TiO_2, CMCD–Fe_3O_4–TiO_2 shows accelerated DBP degradation within 1 h	[77]
DBP	$gC_3N_4/Bi_2O_2CO_3$; g-$C_3N_4/BiOCl$	Halogen tungsten lamp	DBP is removed up to 60% within 3 h	[78]
DEP	Nanorod ZnO/SiC nanocomposite	UV and visible lamp	DEP degradation was achieved up to 90% within 1h	[79]

5. Removal of Phenol and Phenolic Compounds

Phenol and phenolic compounds are primary toxic water pollutants; thereby requiring effective remediation techniques to reduce their harmful effects on both humans and the environment. Numerous studies were carried out in recent times to understand and optimize the degradation of phenol and phenolic compounds. Accordingly, Hassan et al. (2020) [80] report an efficiency of 90% upon degrading phenol using acetylacetonate, rather than graphene nanocomposites, as the photocatalyst, assisted by visible light irradiation. Likewise, Tang et al. (2021) [81] report 100% removal of phenol from different water sources, including sewage wastewaters, upon using a bismuth-doped TiO_2-based photocatalyst. For better effectiveness in environmental degradation, the use of the Z-scheme photocatalytic system is widely encouraged. Supporting this, Xu et al. (2021) [82] note enhanced photocatalytic degradation of phenolic compounds carried out using a Z-scheme charge transfer, with $LaFeO_3/WO_3$ as the photocatalyst. In recent times, several researchers focused on advanced oxidation processes (AOPs) for the complete mineralization of phenols, citing its rapid rate of degradation with the active participation of the hydroxyl radical, and phenol degrading into CO_2 and water, instead of any harmful by-products. The process associated with heterogeneous photocatalysis is a widely recognized AOP and requires (i) a semiconductor photocatalyst, (ii) a light energy (UV or visible or solar) source, and (iii) an electron donor or hole acceptor. In this process, hydroxyl radicals are generated upon producing sufficient charge carriers (i.e., electron-hole pair) by supplying energy greater than the bandgap of the semiconductor photocatalyst using the light energy source [83,84].

Specifically, titanium dioxide (TiO_2) is the commonly preferred and highly performing photocatalyst amongst ZnO, CuO, and β-Ga_2O_3, for degrading phenols under the influence of UV light irradiation, due to its non-toxicity, photo-stability, cost-effectiveness, inertness towards chemical and biological systems, and insolubility [85]. Moreover, UV irradiation on a lab-scale can be efficient; however, it is not recommended for commercial and large-scale degradation of phenol, due to a lack of feasibility and cost-effectiveness [85].

In addition, identifying an efficient, yet sustainable, source for UV light is very challenging, as sunlight itself contains only a fraction of UV light (4% of solar spectrum) compared to visible light (46% of solar spectrum) [86]. Hence, photocatalysts responding to sunlight and any visible light must be developed for degradation, and this is achieved by modifying existing photocatalysts using simple, known techniques such as doping, composite semiconductors, dye sensitization, and synthesizing novel, undoped, single-phase mixed oxide photocatalysts [87].

Furthermore, adding dopants such as iodine, nitrogen, sulfur, praseodymium, and iron with TiO_2 photocatalysts improves the photoresponses of the latter into the visible spectrum, thus, making the degradation of phenol highly viable using visible light [88]. For composite semiconductors, a large bandgap semiconductor is coupled with a small bandgap semiconductor, with a more negative conduction band level, thereby allowing the injection of conduction band electrons from the small bandgap semiconductor for better charge carrier separation, as shown in Figure 5. A few examples of composite photocatalysts proven effective in degrading p-nitro phenols under visible light include Co_3O_4, $Bi_4O_5I_2$, and Bi_5O_7I [89]. Chowdhury et al. [90,91] showcase effective phenol degradation using an eosin Y-sensitized Pt-loaded TiO_2 photocatalyst; Qin et al. [92] report the degradation of 4-chlorophenol using an N719 dye-sensitized TiO_2 photocatalyst. Likewise, 4-nitrophenol is degraded upon using two different photocatalysts, namely, (i) Cu(II)-porphyrin and (ii) Cu(II)-phthalocyanine-sensitized TiO_2, under visible light irradiation. It is worth mentioning that dyes are active in visible light by nature, but become excited upon illumination by any other light source. The degradation of various phenols and their derivatives, using nanoparticle-based heterogeneous catalysts, is shown in Table 4.
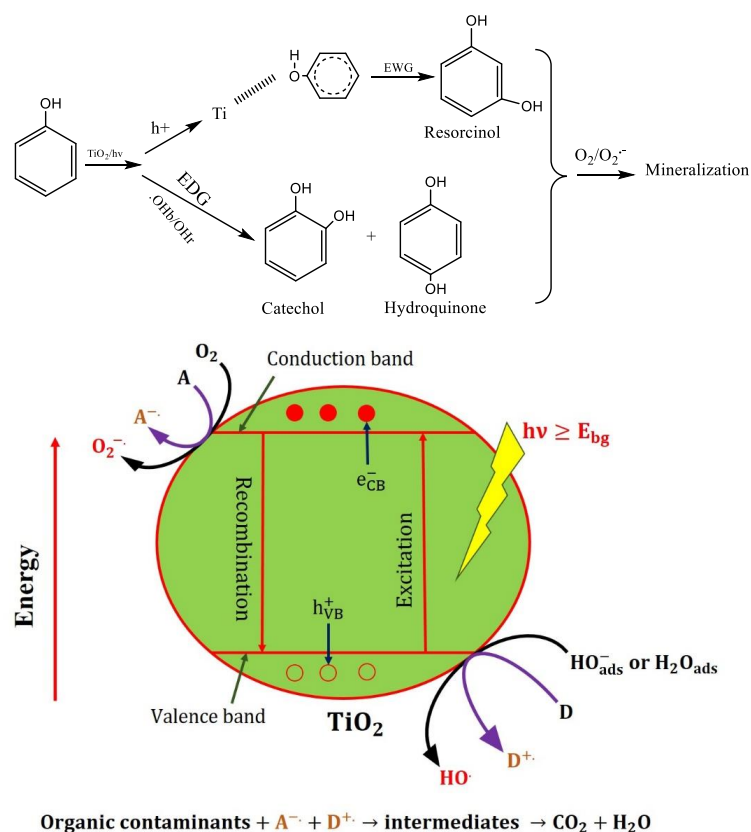

Figure 5. Photocatalytic degradation of phenol and its derivatives.

Table 4. Degradation of various phenols and their derivatives using nanoparticle-based heterogeneous catalysts.

Phenol and Phenolic Compounds	Photocatalyst and Light Source	Degradation Efficiency	References
Phenol	TiO_2/CMK-3, UV lamps, 150 min	74%	[93]
Phenol	PAN-CNT/TiO_2–NH_2, UV lamp, 7 min	99%	[94]
Phenol	UV/TiO_2 and Vis/N, C–TiO_2, 60 min	76%	[95]
Phenol	NIR irradiation, Nd-Er co-doped tetragonal $BiVO_4$, 150 min	96%	[96]
Phenol	Visible light, N-BiOBr/$NiFe_2O_4$-15 nanocomposite, 60 min	87.5%	[97]
Bisphenol A	UV-light, $BiVO_4$/CHCOO(BiO), 5h	99%	[98]
Phenol	$BiVO_4$/carbon, Xenon lamp, 5 h	80%	[99]
Phenol	$Bi_4V_2O_{10}$/$BiVO_4$, Xenon lamp, 60 min	95%	[100]
Phenol	CdS/TiO_2 Xenon lamp, 3 h	78%	[101]
4-chlorophenol	TiO_2/Zr, Xenon lamp, 4 h	95%	[102]
4-fluorophenol	Ag_3PO_4/$H_3PW_{12}O_4$ Xenon lamp,10 min	100%	[103]
Phenol	Au/BiOBr/Grapheme, Xenon lamp, 180 min	64%	[104]
Phenol	α-Fe_2O_3 nanorod/rGO, visible light, 120 min	67%	[105]
Phenol	$Bi_7O_9I_3$/rGO, visible light, 150 min	78.3%	[106]
Phenol	AgBr/BiOBr/graphene, visible light, 120 min	98%	[107]
Phenol	ZnO/TiO_2, visible light, 160 min	100%	[108]
4-chlorophenol	RGO/$CaFe_2O_4$/Ag_3PO_4, visible light, 160 min	90%	[109]
2,4 dichlorophenol	Graphene/ZnO/Co_3O_4, visible light, 150 min	91%	[110]

6. Removal of Drugs and Antibiotics and Their Derivatives

In general, drugs are discharged as pollutants into the atmosphere in form of excreta from individuals and animals, in addition to effluents discharged from pharmaceutical industries. Specifically, these drug molecules have adverse effects on the ecosystem, affecting aquatic life in terms of their lifecycle, growth retardation, and a reduction in friendly microbes. Apart from these impacts, excessive consumption of these drugs causes kidney problems in humans, in addition to increasing the immunity of pathogens towards these drugs. Moreover, these antibiotics form unknown complex compounds with heavy metals or other organic pollutants. To understand their severity, numerous researchers

focus on degrading these antibiotics and drugs using photocatalysts; recently, the use of TiO_2 and Au-infused TiO_2 nanoparticles can be used to degrade a total of eight antibiotics with higher conversion efficiency [111]. Though many studies report 100% removal efficiency, Bekkali et al. (2017) [112] report 80% removal efficiency for sulfadiazine, amoxicillin, and anthramycin, upon using photosensitive TiO_2 irradiated using UV light. In another study, the effect of degradation on natural and synthetic antibiotics is studied, and Mohammad et al. (2020) [94] report the degradation efficiency, upon using immobilized TiO_2 under UV light, as 92.81% for synthetic, and 86.57% for natural, ciprofloxacin. Another catalyst, ZnO, is also used in UV-irradiated photocatalytic degradation, where better efficiencies are reported for prolonged reaction durations [113]. They are encouraged for large and commercial-scale applications and these catalysts were used for degrading sulfamethazine in different shapes, forming flower-shaped, tetra-needle-shaped, and regular ZnO nanoparticles, with T-ZnO reporting 100% conversion [113]. Likewise, 20 ppm of levofloxacin was degraded under visible light irradiation using $BiVO_4$, and reported 85% efficiency within 90 min of the conversion [114]. Another set of drug pollutants includes antineoplastic drugs used in anti-cancer treatments, which enter water bodies through excretion and effluent discharge from pharma industries, thus, increasing the levels of toxicity [115]. The schematic representation of photocatalytic degradation of pharmaceutical pollutants is shown in Figure 6.
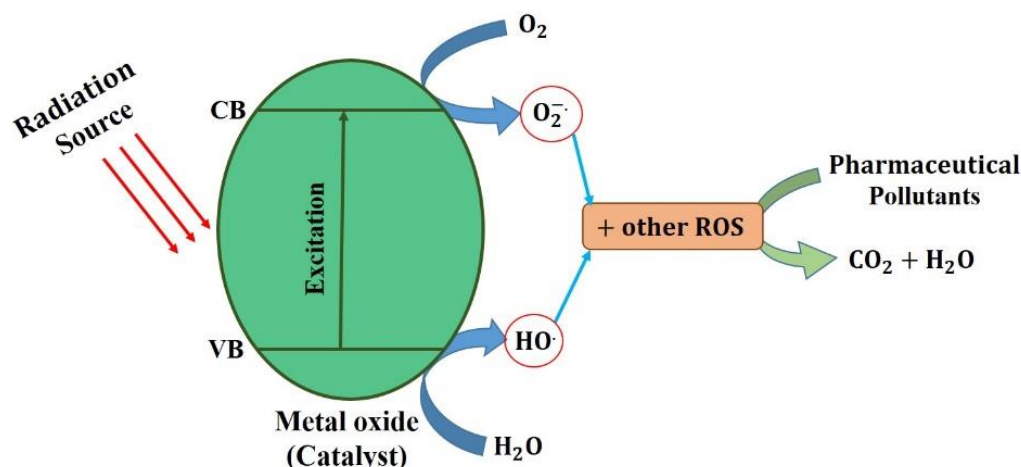

Figure 6. Photocatalytic degradation of pharmaceutical pollutants.

Interestingly, Hank Hui-Hsiang Lin and Angela Yu-Chen Lin (2013) [116] comment that high conversion efficiency is reported for photocatalysis upon degrading 5-fluorouracil and cyclophosphamide via a UV/TiO_2-irradiated light source. UV–visible light-irradiated photocatalytic degradation was carried out on a common antibiotic named tetracycline, using iron oxide nanoparticles as the potential photocatalyst [117]. Similarly, double-shelled $ZnSnO_3$ hollow cube nanoparticles were then used in degrading ciprofloxacin and sulfamonomethoxine [118]. Some of the commonly used photocatalysts for degrading these antibiotics include $Ag_3PO_4/Ag/BiVO_4$ Z-scheme photocatalysts [119], g-C_3N_4-doped porous carbon nitride [120], $Ag_l/Bi_{12}O_{17}C_{l2}$, $Ag_2Mo_2O_7/MoS_2$ Z-scheme 1D/2D photocatalysts [121], WO_3/gC_3N_4 Z-scheme photocatalysts [122], and $BiOCl/g-C_3N_4/Cu_2O/Fe_3O_4$ [123]. It is worth mentioning that, in some cases, the simultaneous degradation of antibiotic pollutants and generation of hydrogen is noted. In certain cases, non-toxic and less harmful antibiotics were also remediated; supporting this, naproxen, a common non-steroidal anti-inflammatory drug, was degraded using photocatalysts such as g-C_3N_4, carbon quantum dots, and single-atom dispersed silver [120]. Similarly, a carbon nitride-based heterojunction photocatalyst was used to degrade ibuprofen, while TiO_2 remains highly effective in degrading carbamazepine, diclofenac, and ibuprofen upon irradiation using a visible light source [124]. The degradation of various drugs and antibiotics, using nanoparticle-based heterogeneous catalysts, is shown in Table 5.

Table 5. Degradation of various drugs and antibiotics using nanoparticle-based heterogeneous catalysts.

Pollutant	Photocatalyst	Light Source	Drugs and Antibiotics Degradation Efficiency	References
Acetaminophen Levofloxacin	CdS sub-microspheres	Visible light, 4 h	85% 70%	[125]
Paracetamol	TiO_2–graphite composites	UV lamp, 60 min	100%	[126]
Doxycycline	$BiOBr/FeWO_4$	Xenon light, 60 min	90.4%	[127]
Tetracycline hydrochloride	$CdTe/TiO_2$	Halogen lamp, 60 min	78%	[128]
Tetracycline Fe-based	Metal-organic frameworks	Xenon lamp, 180 min	96.6%	[129]
Tetracycline hydrochloride	$ZnFe_2O_4$ porous hollow cube	Xenon lamp, 60 min	84.08%	[130]
Tetracycline	$ZnWO_4-x$ nanorods	Xenon lamp, 80 min	91%	[131]
Ofloxacin	TiO_2	Visible light, 60 min	98%	[132]
Norfloxacin	TiO_2	Visible light, 60 min	99%	[132]
Ciprofloxacin	TiO_2	Visible light, 120 min	91%	[132]
Nitrofurantoin	$Nd_2Mo_3O_9$	Tungsten incandescent, 45 min	99%	[133]

7. Removal of Dyes and Their Derivative

Dyes are a group of chemicals used as coloring agents in the textile industry, but when left untreated, these chemicals contaminate the aquatic ecosystem, causing mutation and sterility in aquatic organisms. Presently, numerous conventional techniques are practiced in wastewater treatment, but are found to be ineffective; however, the use of nanoparticle-based heterogeneous photocatalysts reports better degradation efficiency [134]. Confirming this, the rate of degradation of methylene blue using SnO_2 as a photocatalyst, assisted with UV light irradiation, has a maximum efficiency of 80–97%, along with high catalytic stability and reusability [135]. Another study uses TiO_2/WO_3-coated magnetic nanoparticles for degrading sixteen organic dyes, and notes a rapid rate of degradation, with complete decolorization noted in the case of ten dyes upon irradiation in direct sunlight [136]. Another type of photocatalyst includes copper-based nanoparticles, which exhibit effective degradability of organic dyes, as proven by Rao et al. (2019), who report 98% efficiency upon degrading Reactive Black dye using copper oxide nanorods [30]. Furthermore, these nanoparticles report similar degradation efficiencies upon remediating methyl orange, methylene blue, and Congo red, simultaneously [137]. Other photocatalytic degradation of dyes includes the degradation of rhodamine B using $Cu/Cu(OH)_2$ nanoparticles [137], the degradation of methyl orange using CdS/CuS nanoparticles [138], the degradation of methylene blue via Hummers' method using reduced graphene oxide doped with copper nanoparticles [139], the degradation of methyl red, methyl orange, and phenyl red using biologically prepared copper nanoparticles [140], and the degradation of methyl orange using graphene oxide-doped $CuO-Cu_2O$ and Cu_3N/MoS_2 [141]. The degradation of various dyes, using nanoparticle-based heterogeneous catalysts, is shown in Table 6.

Table 6. Degradation of various dyes using nanoparticle-based heterogeneous catalysts.

Dye	Photocatalyst	Light Source	Results	References
Methylene blue	ZnO/CuO	Visible lamp, 25 min	96.57%	[142]
Methylene blue Rhodamine B	Carbon/BiVO$_4$	Xenon light, 180 min	95% 80%	[99]
Rhodamine B acid Chrome blue	CdS-reduced graphene oxide	Xenon light, 60 min	97.2% 65.7%	[143]
Rhodamine B	WO$_3$	Metal halide lamp, 180 min	95%	[144]
Rhodamine B	rGO/RP-MoS$_2$	Xenon light, 30 min	99.3%	[145]
Acid Black 1 dye	TiO$_2$–graphene	Visible light, 60 min	96%	[146]

8. Factors Affecting the Degradation of Photocatalysis

The main factors that influence the photocatalytic degradation of organic pollutants are (i) the load of the catalyst, (ii) doping (iii) pH, (iv) light intensity, and (v) the lifetime and regeneration of the photocatalyst. The efficiency of the photocatalytic degradation of pollutants is highly dependent on the number of operational parameters. Several studies show the enhancement of the efficiency of the photocatalytic degradation of organic pollutants. In this review paper, the major factors influencing the efficiency of the photocatalytic degradation of pollutants are discussed below.

8.1. Catalyst Loading

The load of the catalysts is one of the key factors that influence the photocatalytic degradation of pollutants. Due to the increase in the active sites, the rate of the photocatalytic degradation of organic pollutants increases with photocatalysts dosage [147–151]. This is because when the photocatalysts are irradiated in the presence of light, it results in the formation of hydroxyl radical ions. When the concentration of the photocatalyst is low, it affects the efficiency of the photocatalytic degradation of pollutants, since more light is transmitted into the photocatalytic reactor, and less transmitted radiation is utilized in the degradation of pollutants [152,153]. The optimization process of the catalyst load is one of the major parameters that impact the whole catalytic process and its efficiency. Most of the researchers concentrated on the process optimization parameters of the photocatalytic degradation of pollutants. Based on the extensive literature survey, it is found that increasing the catalyst load increases the degradation of pollutants, which proportionally produces more hydroxyl ions and positive holes, and absorbs more photons, due to the availability of a large number of catalyst surfaces. As a result, this increases the degradation rate at a higher concentration, causing interference of the light to penetrate the solution, which restricts the light in passing through the solution [154,155]. This reduces the degradation percentage, and the phenomenon is known as the scattering of light [156]. In some cases, a certain amount of catalyst loading results in solution turbidity and, thus, blocks the UV radiation for the reaction to proceed, and finally decreases the degradation rate of the pollutants [157–160]. Beyond the optimum amount of catalysts, loading may affect the pollutant degradation rate, which is due to the increase in the opacity of the photocatalyst suspension. Increasing the light scattering and infiltration depth of the photons results in diminishing, meaning fewer photocatalysts may be activated, and also results in the agglomeration of nanoparticles at a higher concentration of photocatalysts. The agglomeration of nanoparticles occurs due to the activation of a lower number of surface-active sites during the photocatalytic degradation process, and also results in the deactivation of

the activated molecules, leading to the collision of the activated molecules in the ground state [161]. Table 7 describes the dependency of the photocatalytic activity on the catalysts loading and their conversion efficiency.

Table 7. Dependency of the photocatalytic activity on the catalysts loading and their conversion efficiency.

Pollutant	Photocatalyst	Catalyst Load	Efficiency	Reference
Sulfamethoxazole	$BiVO_4/CHCOO(BiO)$	1 g/L	85%	[98]
Methylene blue	CuO/ZnO	1 g/L	96.57%	[142]
Methylene blue	$BiVO_4/carbon$	1.0 g/L	95%	[99]
Rhodamine B	CdS-reduced graphene oxide	0.4 g/L	97.2%	[143]
Rhodamine B	$Bi_4V_2O_{10}/BiVO_4$	1 g/L	100%	[100]
4-fluorophenol	$Ag_3PO_4/H_3PW_{12}O_{40}$	3 g/L	100%	[103]
Methyl orange		3 g/L	100%	
Rhodamine B	WO_3	1 g/L	95%	[144]
Rhodamine B	$RP\text{-}MoS_2/rGO$	0.4 g/L	99.3%	[145]
4-chloro Phenol	$ZrTiO_2$	0.1 g/L	95%	[102]

8.2. Doping

The efficiency of the photocatalyst can be increased by doping in the following ways: bad gap narrowing; oxygen vacancies; formation of impurity energy levels; unique surface area; electron trapping, etc. [162]. Generally, a catalyst with smaller bandgap energy is an effective photocatalyst to produce more electron-hole pairs. The doping process prevents the recombination of electrons and holes, and enhances photocatalytic activity by trapping the photoinduced electrons [163]. The incorporation of dopant ions in the catalysts reduces the radius of lattice ions and lattice space. Similarly, dopant ions are incorporated into the catalyst crystal lattice to enhance the electronic property of the photocatalysts, and also to improve the light absorption ability in the visible light region [164]. Increasing the optimum level by adding a dopant to the catalyst reduces the photocatalytic activity. Narrowing the charge space area increases the recombination of higher dopants than the optimum level, reducing the surface area. The dopant then turns to the recombination center, which ultimately decreases the activity of the photocatalyst [165]. In the case of TiO_2, adding too much dopant reduces the thermal stability of TiO_2, which causes phase transformation of TiO_2 anatase to turn to rutile. A higher level of doping forms clusters in the surface of the photocatalyst, which decreases the photocatalytic activity by reducing the light penetration into the actual photocatalyst surface, and shields the surface area, which causes agglomeration [162]. However, some reports suggest that adding a dopant to the surface increases the mesoporous structure of the catalyst. In the case of using a noble metal as a dopant, which separates the electron and hole pair by the phenomenon of surface plasmon resonance under visible light, and also increases the adsorption of the pollutant onto the surface of the catalyst, the traps are formed by the noble metal when it acts as a dopant, which reduces the recombination by trapping. In metals, it increases the lifetime of the catalyst by preventing corrosion, due to the organic metal reaction with the surface of the photocatalyst [166]. Doping controls the specific surface area, morphology, crystallinity of the photocatalyst, and particle size. There are different types of dopants, such as anionic and cationic dopants; adding anionic dopants makes the process simple by working under visible light with better stability, and gives a better yield under the visible region compared to UV radiation [166]. Nitrogen, sulfur, phosphorous, carbon, and fluorine are the anionic species that form impurity energy levels near the valence band, and give greater efficiency. In both substitution and interstitial mode, nitrogen is incorporated into the lattice of the photocatalyst. By adding activated carbon, the surface area of the

catalyst increases and its efficiency increases. The crystalline property of the semiconductor photocatalyst is reduced when adding a dopant to the surface; adding large amounts of cerium and nitrogen decreases the crystallinity. Consequently, Chen et al. [167] study the composition of rutile, increasing the doping concentration by reducing the thermal stability of anatase. This results in the phase transformation of anatase into rutile. In the case of mesoporous nanoparticles, doping materials decrease the photocatalytic activities, due to the surface site being blocked by doping material. Under visible light irradiation, higher photocatalyst efficiency is achieved by introducing impurity energy levels, which narrow the bandgap and form oxygen-deficient sites and more electron-hole pairs [168]. The photocatalytic activity of the prepared catalyst depends on how well the recombination of the photoinduced hole–electron pairs is prevented. Doping prevents the recombination of electrons and holes and improves photocatalytic activity by trapping the photoinduced electrons. By adding the dopant substitutionally and interstitially to the photocatalyst, degradation of organic pollutants is enhanced [169]. Table 8 describes the removal of various pollutants using different types of doped photocatalysts.

Table 8. Removal of various pollutants using different types of doped photocatalysts.

Pollutant	Light Source	Dopant Material	Removal Efficiency	Reference
Methylene blue	Visible light	Ag–TiO_2	96%	[170]
Rhodamine B	Solar light	CeO_2-doped TiO_2	99.8%	[171]
POME	Visible light	Ag–TiO_2	26.77%	[172]
Phenol	UV–Visible light	Ag–TiO_2	Up to 50%	[173]
Malachite green	UV–Visible light	Fe–TiO_2	75.81%	[174]
Nitrobenzene	UV light	Fe–TiO_2	99.7%	[175]
Reactive red-198	Visible light	Cu–TiO_2	13%	[176]
Bisphenol A	Visible light	Cu–TiO_2	77%	[177]
Methylene blue	Visible light	Ni–TiO_2	63%	[178]
Phenol	Visible light	Co–TiO_2	81.72%	[179]
Rhodamine B	Solar light	Bi–TiO_2	97%	[180]
4-Chlorophenoxy acetic acid	Visible light	N–TiO_2	73%	[181]
Phenol	Visible light	N–TiO_2	Up to 25%	[182]
Phenol	Visible light	B–TiO_2	12.33%	[183]
Phenol	UV light	F–TiO_2	78%	[184]

8.3. pH of the Solution

In the photocatalytic degradation of pollutants in wastewater, the pH of the wastewater significantly influences the photocatalytic efficiency process. Several studies report on the effect of pH on the photocatalytic reaction. In the photocatalytic degradation process, the pH of the reaction mixture mainly depends on the catalyst surface charge and the chemical-charged particle present in the samples. In the case of wastewater treatment, the pH is mainly dependent on the charge of the photocatalyst, the size of the aggregates, and the position of the conductance and valence bands [185]. If the surface charge and adsorbate have similar charges, resulting in a decrease in the rate of the photodegradation process, the pH of the solution should be maintained to stabilize the photocatalytic degradation of the pollutant [186,187]. It is reported that ZnO with SnO_2 nanoparticles shows better catalytic properties at a neutral pH than at acidic (pH = 4) or alkaline (pH = 10) pH levels [188]. Similarly, if the material's surface charge opposes the adsorption process

because the adsorbate contains the same charge, the pH conditions reveal the optimal adsorption [189]. The photocatalyst Mg–ZnO–Al$_2$O$_3$ was observed to degrade 20 mg/L caffeine solution at pH 9.5 [23] . According to the researchers, changes in the surface charge, and the ionization of caffeine molecules, increase the generation of hydroxyl radicals and enhance the photocatalytic degradation of pollutants under varied pH conditions of the reaction substrate [190]. Generally, pH parameters include many factors, such as decomposition, and the non-favorable adsorption dissolution of the photocatalyst [191]. However, the pH of the solution is 9 in the optimal condition for the photodegradation of the Acid Black 1 dye solution with a photodegradation efficiency of up to 90.1% using a ZnO photocatalyst [24]. The removal effectiveness is lower at acidic pH levels, due to photocatalyst dissolution. As the photocatalyst surface charge is inversely proportional to the solution charge, the pH solution must be evaluated [191]. It was recently reported that at a lower pH level, the maximum oxidizing capacity of titanium-based photocatalysts lowers the rate of the reaction, due to the presence of excess H$^+$ in the reactant solution. To enhance the photocatalytic degradation of pollutants, pH optimization is very important, in order to determine the rate of the reaction [192]. Kiomars Zargoosh et al. (2020) [193] report the use of a nanocomposite of CaAl$_2$O$_4$:Eu^{2+}:Nd^{3+} photocatalyst for the removal of methylene blue dye, by varying the pH of the solution from 7 to 10. At a higher concentration of hydroxyl ions under alkaline conditions, the rate of degradation is faster than in acidic conditions. At pH values higher than 10, the reduction in the removal efficiency may be due to the inactivation of the photocatalyst [193]. A. F. Alkaim et al. (2014) [194] report that photocatalytic dye degradation efficiency is enhanced by varying the pH from 4 to 11. The photodegradation of pollutants is enhanced at pH 6 when using TiO$_2$ as a photocatalyst, as shown in Figure 7a. Generally, dye pollutants are negatively charged in the base medium, and their adsorption may also be affected by an increase in the density of the Ti–O group on the surface. This type of mechanism always occurs, due to coulombic repulsion of the dye pollutant. Similarly, changing the pH from 6 to 7 demonstrates a decrease in the photocatalytic degradation of dye in both acidic and alkaline pH, whereas at high pH values the hydroxyl radicals are rapidly scavenged, and they do not have the opportunity to react with dye pollutants [195]. Using zinc oxide as a photocatalyst significantly enhances the photodegradation of dye at the high pH of 11, whereas at a low pH, the photodecomposition of ZnO into Zn^{2+} in acidic, neutral, and alkaline conditions results in the formation of hydroxyl radical ions, as shown in Figure 7b. In the case of Co$_3$O$_4$, the photocatalytic dye degradation efficiency is reduced at a high pH of 11. The same trend is observed in a CdS photocatalyst, as shown in Figure 7c,d. Based on the above results, it is concluded that the pH of the reactant solution plays an important role in the degradation of pollutants [196].

8.4. Light Intensity

The light intensity affects the efficiency of photocatalysts. When the intensity of the light source is low, between 0–20 mW/cm^2, the rate of the reaction increases in light intensity. At the middle range of light intensity (25 mW/cm^2), the rate of the reaction depends on the square root of the light intensity, and at high intensities the rate of the reaction is independent of light intensity. At low light intensity in the photocatalytic reaction, an electron-hole pair separates and then recombines, which reduces the formation of free radicals and results in the degradation of organic pollutants. Neppolian et al. (2003) [150] report the photocatalytic degradation of Reactive Yellow 17, Reactive Red 2, and Reactive Blue 4 dyes using titanium dioxide photocatalyst, under solar (or) UV radiation as a light source. Compared with solar radiation, UV radiation is more effective in the degradation of the selected dyes [150]. The energy of the UV radiation is large compared to the bandgap energy of the catalysts. The reason behind this is a recombination of the electron-hole pair, which is completely avoided in the presence of a UV source. Using sunlight as a source of light energy in the photocatalytic degradation of pollutants means that only 5% of the total radiation energy is used for the bandgap excitation of electrons. Hence, the percentage

degradation is found to be less in solar radiation compared with the UV source of photocatalytic pollutant degradation [196]. Hung and Yuan (2000) [197] study the effect of light intensity on the photocatalytic degradation of pollutants. The light intensity ranges from 215 to 586 $\mu W/cm^2$, increasing the degradation efficiency of the pollutants with the increasing light intensity. In the study of Chanathaworn et al. (2012) [198], the intensity of the black light lamp is varied between the ranges of 0–114 W/m^2, and the impact of light intensity radiation efficiency on the degradation of the rhodamine B pollutant is analyzed. Based on the experimental results, when the intensity of the light source increases, it enhances the efficiency of the pollutant degradation. Under three different light intensities (1.24 mW/cm^2, 2.04 mW/m^2, and 3.15 mW/m^2) the decolorization of acid yellow 17 degradation is studied, using a photocatalyst to enhance the pollutant efficiency [199]. For the enhancement of the degradation rate of the pollutant using different types of photocatalyst, the light intensity may be increased from a lower frequency to a higher frequency [200,201]. Similarly, Rao et al. (2004) demonstrate that the rate of the photocatalytic degradation of acid orange 7 dye pollutant is increased 1.5 times in a peak sunlight source compared to the artificial UV light sources [202]. An overall observation of the stated research results is that the wavelength of the irradiation affects the efficiency of the photocatalytic degradation process. The scientific evidence clearly states that a shorter wavelength of irradiation stimulates the electron–hole generation, and subsequently enhances the efficiency of the catalyst [203].
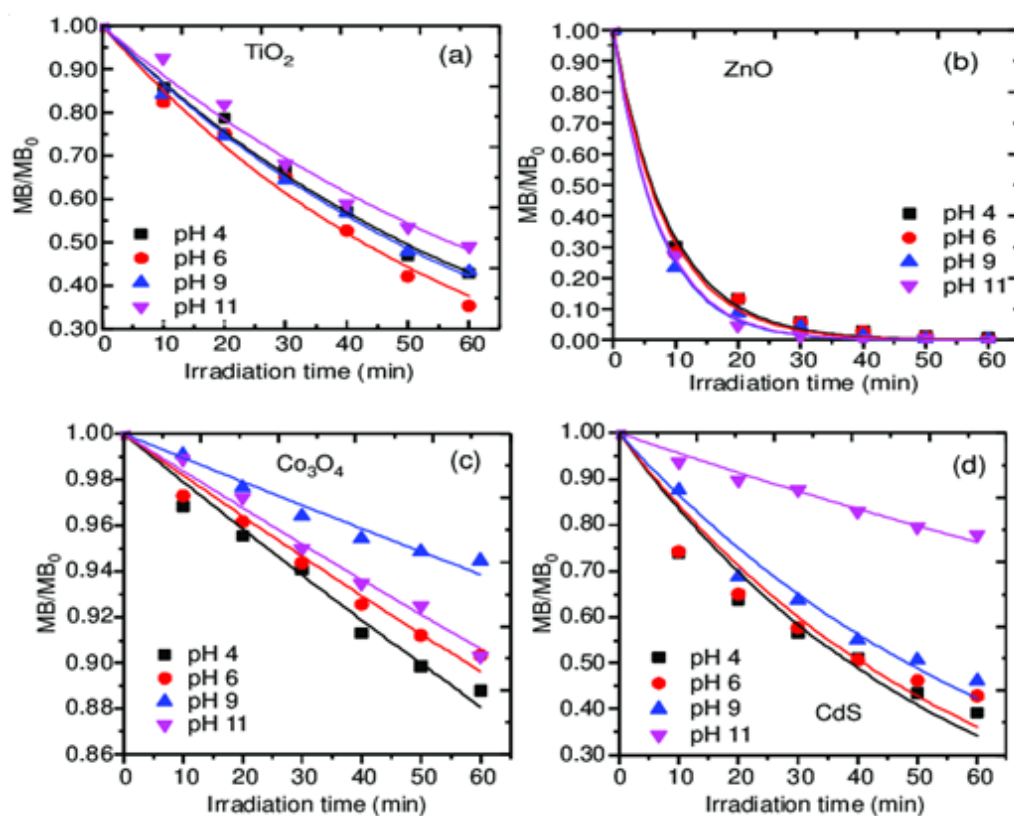

Figure 7. Photocatalytic degradation of methylene blue in the presence of different pH levels of the solution; (**a**) TiO_2, (**b**) ZnO, (**c**) Co_3O_4, and (**d**) CdS [194].

8.5. Lifetime and Regeneration of Photocatalyst

The lifetime and regeneration of the photocatalyst are important to ensure the efficiency and the quality of the synthesized catalyst. The photocatalytic degradation efficiency affects the lifetime and regeneration of the photocatalyst. The quality of the photocatalyst is important for the photocatalytic degradation of the contaminants, as it mainly depends on the process of the catalyst synthesis, dopants, and selection of the catalyst. Several catalyst performances reduce after a certain cycle, due to their corrosion properties. Photocatalyst

must maintain good stability and reusability, which is an essential factor for the pollutant degradation process. Most photocatalysts are deactivated after several cycles of the reaction process. Many factors are responsible for the deactivation of the photocatalysts, such as the loss of photocatalyst mass, especially during the washing/purification process. It has been reported that some amounts of rod-shaped ZnO stacking occur on Cu_2O/Ag_3PO_4 during filtration [204]. Leaching of dopants usually occurs during the reaction due to photoetching [205]. A synthesized ZnO catalyst undergoes photodecomposition after three cycles in the degradation of rhodamine B, and the nanosized photocatalyst has a high porosity surface, because of the deactivation of catalysts. The highly stable, novel photocatalyst $Ag_2Nb_4O_{11}$ has 40 times the reusable capacity for the degradation of rhodamine B, methylene blue, and methyl orange [206]. The researchers discovered that the methylene blue of organic intermediates is adsorbed on the photocatalyst surface during every cycle [207]. In summary, the strength, durability, and stability of the catalyst are based on the reaction parameters involved in the photocatalytic degradation process. This is to ensure that the prepared catalyst has high reusability, and recycling the ability minimizes the cost of the process.

9. Conclusions

The review mainly focused on photocatalysis technology used to solve environmental problems. In the present paper, we explained the degradation of pollutants present in wastewater. The major pollutants present in wastewater are polybrominated diphenyl ether and its derivatives, phthalates and its derivatives, phenolic compounds, drugs and antibiotics, and dye compounds, etc. These compounds were effectively removed using nanomaterials in the presence of light. The study shows that metal oxides of titanium, barium, copper, zinc, lanthanum, nickel, silver, cerium, iron, and others are effectively used as photocatalysts in the removal of various pollutants. The removal of pollutants from wastewater is based on the reaction conditions in the presence of various types of photocatalysts. A potential photocatalyst is capable of degrading all types of pollutants with higher efficiency, but using photocatalysts has some disadvantages. The recombination rate is high and it works efficiently under UV light irradiation, but a catalyst that works in the visible light to utilize the solar energy without any restraint is needed. This can be rectified by doping and the Z-scheme effect, as both of these effectively rectify this in the various types of heterogeneous nanoparticle-based photocatalysts with common photocatalytic errors such as higher recombination rate, large bandgap, and the inability to harvest visible light. Generally, titanium, copper, zinc, iron, and all other compounds are also effective in degradation, with metal-doping enhancing the degradation efficiency. The efficiency of the photocatalyst is mainly based on fundamental factors such as pH, doping, catalysts loading, light intensity, and stability. These factors have a significant part in the degradation of pollutants. The major functions of these parameters, and their impact on the rate of photocatalytic degradation efficiency, were elaborated in detail in the present paper. Finally, a photocatalyst is cheap and more stable compared to other conventional catalysts, as well as being economical and environmentally friendly. With the growth and extension of the research, photocatalysis technology was extended to many fields, such as energy, health, environment, pollution control, and the synthesis of value-added chemicals. As a result, the relevance of photocatalysis to human life is increasing steadily. The grand challenge of photocatalysis today is to further expand the practical application of photocatalytic technology in the industrial field.

Author Contributions: C.S.: Conceptualization, Writing—original draft, S.V.: Data curation, Visualization, and Validation. E.L.: Funding acquisition. S.S.: Conceptualization, Writing—review & editing. R.J.: Conceptualization, Writing—original draft. All authors have read and agreed to the published version of the manuscript.

Data Availability Statement: All relevant data are within the paper.

Conflicts of Interest: The authors have no conflict of interest to declare regarding the publication of this work.

References

1. Khan, I.; Saeed, K.; Khan, I. Nanoparticles: Properties, applications and toxicities. *Arab. J. Chem.* **2019**, *12*, 908–931. [CrossRef]
2. Tharani, K.; Jegatha Christy, A.; Sagadevan, S.; Nehru, L.C. Photocatalytic and antibacterial performance of iron oxide nanoparticles formed by the combustion method. *Chem. Phys. Lett.* **2021**, *771*, 138524. [CrossRef]
3. Sibhatu, A.K.; Weldegebrieal, G.K.; Sagadevan, S.; Tran, N.N.; Hessel, V. Photocatalytic activity of CuO nanoparticles for organic and inorganic pollutants removal in wastewater remediation. *Chemosphere* **2022**, *300*, 134623. [CrossRef] [PubMed]
4. Sibhatu, A.K.; Weldegebrieal, G.K.; Sagadevan, S.; Tran, N.N.; Hessel, V. Synthesis and Process Parametric Effects on the Photocatalyst Efficiency of CuO Nanostructures for Decontamination of Toxic Heavy Metal Ions. *Chem. Eng. Processing-Process Intensif.* **2022**, *173*, 108814. [CrossRef]
5. Zularisam, A.W.; Ismail, A.F.; Salim, M.R. Behaviours of natural organic matter in membrane filtration for surface water treatment—A review. *Desalination* **2006**, *194*, 211–231. [CrossRef]
6. Zazouli, M.A.; Kalankesh, L.R. Removal of precursors and disinfection by-products (DBPs) by membrane filtration from water: A review. *J. Environ. Health Sci. Eng.* **2017**, *15*, 25. [CrossRef]
7. Azimi, A.; Azari, A.; Rezakazemi, M.; Ansarpour, M. Removal of Heavy Metals from Industrial Wastewaters: A Review. *ChemBioEng Rev.* **2017**, *4*, 37–59. [CrossRef]
8. Yagub, M.T.; Sen, T.K.; Afroze, S.; Ang, H.M. Dye and its removal from aqueous solution by adsorption: A review. *Adv. Colloid Interface Sci.* **2014**, *209*, 172–184. [CrossRef]
9. Mousset, E.; Doudrick, K. A review of electrochemical reduction processes to treat oxidized contaminants in water. *Curr. Opin. Electrochem.* **2020**, *22*, 221–227. [CrossRef]
10. Arar, Ö.; Yüksel, Ü.; Kabay, N.; Yüksel, M. Various applications of electrodeionization (EDI) method for water treatment—A short review. *Desalination* **2014**, *342*, 16–22. [CrossRef]
11. Sagadevan, S.; Lett, J.A.; Weldegebrieal, G.K.; Imteyaz, S.; Johan, M.R. Synthesis, characterization, and photocatalytic activity of PPy/SnO$_2$ nanocomposite. *Chem. Phys. Lett.* **2021**, *783*, 139051. [CrossRef]
12. Nida, Q.; Singh, P.; Sabir, S.; Umar, K.; Sagadevan, S.; Oh, W. Synthesis of Polyaniline Supported CdS/CdS-ZnS/CdS-TiO$_2$ Nanocomposite for Efficient Photocatalytic Applications. *Nanomaterials* **2022**, *12*, 1355.
13. Saravan, R.S.; Muthukumaran, M.; Mubashera, S.M.; Abinaya, M.; Prasath, P.V.; Parthiban, R.; Mohammad, F.; Oh, W.C.; Sagadevan, S. Evaluation of the photocatalytic efficiency of cobalt oxide nanoparticles towards the degradation of crystal violet and methylene violet dyes. *Optik* **2020**, *207*, 164428. [CrossRef]
14. Fujishima, A.; Honda, K. Electrochemical Photolysis of Water at a Semiconductor Electrode. *Nature* **1972**, *238*, 37–38. [CrossRef]
15. Reiche, H.; Dunn, W.W.; Bard, A.J. Heterogeneous photocatalytic and photosynthetic deposition of copper on Titanium dioxide and tungsten (VI) oxide powders. *J. Phys. Chem.* **1979**, *83*, 2248–2251. [CrossRef]
16. Xu, Q.; Zhang, L.; Yu, J.; Wageh, S.; Al-Ghamdi, A.A.; Jaroniec, M. Direct Z-scheme photocatalysts: Principles, synthesis, and applications. *Mater. Today* **2018**, *21*, 1042–1063. [CrossRef]
17. Nazim, M.; Khan, A.A.P.; Asiri, A.M.; Kim, J.H. Exploring Rapid Photocatalytic Degradation of Organic Pollutants with Porous CuO Nanosheets: Synthesis, Dye Removal, and Kinetic Studies at Room Temperature. *ACS Omega* **2021**, *6*, 2601–2612. [CrossRef]
18. Gupta, N.K.; Ghaffari, Y.; Kim, S.; Bae, J.; Kim, K.S.; Saifuddin, M. Photocatalytic degradation of organic pollutants over MFe$_2$O$_4$ (M = Co, Ni, Cu, Zn) nanoparticles at neutral pH. *Sci. Rep.* **2020**, *10*, 4942. [CrossRef]
19. Kumar, S.; Sahare, P.D. Photocatalytic activity of Bismuth Vanadate for the degradation of organic compounds. *Nano* **2013**, *8*, 1350007. [CrossRef]
20. Santhosh, C.; Malathi, A.; Daneshvar, E.; Kollu, P.; Bhatnagar, A. Photocatalytic degradation of toxic aquatic pollutants by novel magnetic 3D-TiO$_2$@ HPGA nanocomposite. *Sci. Rep.* **2018**, *8*, 15531. [CrossRef]
21. Saygi, B.; Tekin, D. Photocatalytic degradation kinetics of reactive black 5 (RB 5) dyestuff on TiO$_2$ modified by pretreatment with untrasound energy. *React. Kinet. Mech. Catal.* **2013**, *110*, 251–258. [CrossRef]
22. Vaiano, V.; Sacco, O.; Matarangolo, M. Photocatalytic degradation of paracetamol under UV irradiation using TiO$_2$-graphite composites. *Catal. Today* **2018**, *315*, 230–236. [CrossRef]
23. Elhalil, A.; Elmoubarki, R.; Farnane, M.; Machrouhi, A.; Sadiq, M.; Mahjoubi, F.Z.Z.; Qourzal, S.; Barka, N. Photocatalytic degradation of caffeine as a model pharmaceutical pollutant on Mg doped ZnO-Al$_2$O$_3$ heterostructure. Environ. *Nanotechnol. Monit. Manag.* **2018**, *10*, 63–72.
24. Subash, B.; Krishnakumar, B.; Swaminathan, M.; Shanthi, M. Highly active Zr co-doped Ag-ZnO photocatalyst for the mineralization of Acid Black 1 under UV-A light illumination. *Mater. Chem. Phys.* **2013**, *141*, 114–120. [CrossRef]
25. Tambat, S.; Umale, S.; Sontakke, S. Photocatalytic degradation of metamitron using CeO$_2$ and Fe/CeO$_2$. *Integr. Ferroelectr.* **2018**, *186*, 54–61. [CrossRef]
26. Ateş, S.; Baran, E.; Yazıcı, B. Fabrication of Al$_2$O$_3$ nanopores/SnO$_2$ and its application in photocatalytic degradation under UV irradiation. *Mater. Chem. Phys.* **2018**, *214*, 17–27. [CrossRef]
27. Soares, E.T.; Lansarin, M.A.; Moro, C.C. A study of process variables for the photocatalytic degradation of rhodamine B. *Braz. J. Chem. Eng.* **2007**, *24*, 29–36. [CrossRef]

28. Alafif, Z.O.; Anjum, M.; Ansari, M.O.; Kumar, R.; Rashid, J.; Madkour, M.; Barakat, M.A. Synthesis and characterization of S-doped-rGO/ZnS nanocomposite for the photocatalytic degradation of 2-chlorophenol and disinfection of real dairy wastewater. *J. Photochem. Photobiol. A Chem.* **2019**, *377*, 190–197. [CrossRef]

29. Fathima, J.B.; Pugazhendhi, A.; Oves, M.; Venis, R. Synthesis of eco-friendly copper nanoparticles for augmentation of catalytic degradation of organic dyes. *J. Mol. Liq.* **2018**, *260*, 1–8. [CrossRef]

30. Rao, M.P.C.; Kulandaivelu, K.; Ponnusamy, V.K.; Wu, J.J.; Sambandam, A. Surfactant-assisted synthesis of copper oxide nanorods for the enhanced photocatalytic degradation of Reactive Black 5 dye in wastewater. *Environ. Sci. Pollut. Res.* **2020**, *27*, 17438–17445. [CrossRef]

31. Akram, N.; Guo, J.; Ma, W.; Guo, Y.; Hassan, A.; Wang, J. Synergistic catalysis of $Co(OH)_2$/CuO for the degradation of organic pollutant under visible light irradiation. *Sci. Rep.* **2020**, *10*, 1939. [CrossRef] [PubMed]

32. Zhang, Y.; Zhou, J.; Chen, J.; Feng, X.; Cai, W. Rapid degradation of tetracycline hydrochloride by heterogeneous photocatalysis coupling persulfate oxidation with MIL-53(Fe) under visible light irradiation. *J. Hazard. Mater.* **2020**, *392*, 122315. [CrossRef] [PubMed]

33. Deng, X.; Wang, C.; Yang, H.; Shao, M.; Zhang, S.; Wang, X.; Ding, M.; Huang, J.; Xu, X. One-pot hydrothermal synthesis of CdS decorated CuS microflower-like structures for enhanced photocatalytic properties. *Sci. Rep.* **2017**, *7*, 3877. [CrossRef] [PubMed]

34. Kirankumar, V.S.; Sumathi, S. Photocatalytic and antibacterial activity of bismuth and copper co-doped cobalt ferrite nanoparticles. *J. Mater. Sci. Mater. Electron.* **2018**, *29*, 8738–8746. [CrossRef]

35. Kirankumar, V.S.; Sumathi, S. Structural, optical, magnetic and photocatalytic properties of bismuth doped copper aluminate nanoparticles. *Mater. Chem. Phys.* **2017**, *197*, 17–26. [CrossRef]

36. De Wit, C.A. An overview of brominated flame retardants in the environment. *Chemosphere* **2002**, *46*, 583–624. [CrossRef]

37. Azri, N.; Bakar, W.A.W.A.; Ali, R. Optimization of photocatalytic degradation of polybrominated diphenyl ether on trimetallic oxide $Cu/Ni/TiO_2$/PVC catalyst using response surface methodology method. *J. Taiwan Inst. Chem. Eng.* **2016**, *62*, 283–296. [CrossRef]

38. Wang, R.; Tang, T.; Wei, Y.; Dang, D.; Huang, K.; Chen, X.; Yin, H.; Tao, X.; Lin, Z.; Dang, Z.; et al. Photocatalytic debromination of polybrominated diphenyl ethers (PBDEs) on metal doped TiO_2 nanocomposites: Mechanisms and pathways. *Environ. Int.* **2019**, *127*, 5–12. [CrossRef]

39. Li, Y.; Li, J.; Deng, C. Occurrence, characteristics and leakage of polybrominated diphenyl ethers in leachate from municipal solid waste landfills in China. *Environ. Pollut.* **2014**, *184*, 94–100. [CrossRef]

40. Lei, M.; Wang, N.; Zhu, L.; Tang, H. Peculiar and rapid photocatalytic degradation of tetrabromodiphenyl ethers over Ag/TiO_2 induced by interaction between silver nanoparticles and bromine atoms in the target. *Chemosphere* **2016**, *150*, 536–544. [CrossRef]

41. Lv, Y.; Cao, X.; Jiang, H.; Song, W.; Chen, C.; Zhao, J. Rapid photocatalytic debromination on TiO_2 with in-situ formed copper co-catalyst: Enhanced adsorption and visible light activity. *Appl. Catal. B Environ.* **2016**, *194*, 150–156. [CrossRef]

42. Yao, B.; Luo, Z.; Zhi, D.; Hou, D.; Luo, L.; Du, S.; Zhou, Y. Current progress in degradation and removal methods of polybrominated diphenyl ethers from water and soil: A review. *J. Hazard. Mater.* **2020**, *403*, 123674. [CrossRef] [PubMed]

43. Huang, A.; Wang, N.; Lei, M.; Zhu, L.; Zhang, Y.; Lin, Z.; Yin, D.; Tang, H. Efficient Oxidative Debromination of Decabromodiphenyl Ether by TiO_2-Mediated Photocatalysis in Aqueous Environment. *Environ. Sci. Technol.* **2013**, *47*, 518–525. [CrossRef]

44. Lei, M.; Wang, N.; Zhu, L.; Xie, C.; Tang, H. A peculiar mechanism for the photocatalytic reduction of decabromodiphenyl ether over reduced graphene oxide–TiO_2 photocatalyst. *Chem. Eng. J.* **2014**, *241*, 207–215. [CrossRef]

45. Lei, M.; Wang, N.; Guo, S.; Zhu, L.; Ding, Y.; Tang, H. A one-pot consecutive photocatalytic reduction and oxidation system for complete debromination of tetrabromodiphenyl ether. *Chem. Eng. J.* **2018**, *345*, 586–593. [CrossRef]

46. Guo, S.; Zhu, L.; Majima, T.; Lei, M.; Tang, H. Reductive Debromination of Polybrominated Diphenyl Ethers: Dependence on Br Number of the Br-Rich Phenyl Ring. *Environ. Sci. Technol.* **2019**, *53*, 4433–4439. [CrossRef]

47. Shao, Y.-Y.; Ye, W.-D.; Sun, C.-Y.; Liu, C.-L.; Wang, Q.; Chen, C.-C.; Gu, J.-Y.; Chen, X.-Q. Enhanced photoreduction degradation of polybromodiphenyl ethers with Fe_3O_4-g-C_3N_4 under visible light irradiation. *RSC Adv.* **2018**, *8*, 10914–10921. [CrossRef]

48. Shao, Y.Y.; Ye, W.D.; Sun, C.Y.; Liu, C.L.; Wang, Q. Visible-light-induced degradation of polybrominated diphenyl ethers with Agl-TiO_2. *RSC Adv.* **2017**, *7*, 39089–39095. [CrossRef]

49. Liang, C.; Zhang, L.; Guo, H.; Niu, C.-G.; Wen, X.-J.; Tang, N.; Liu, H.-Y.; Yang, Y.-Y.; Shao, B.-B.; Zeng, G.-M. Photo-removal of 2,2′4,4′-tetrabromodiphenyl ether in liquid medium by reduced graphene oxide bridged artificial Z-scheme system of Ag@Ag_3PO_4/g-C_3N_4. *Chem. Eng. J.* **2019**, *361*, 373–386. [CrossRef]

50. Wei, Y.; Gong, Y.; Zhao, X.; Wang, Y.; Duan, R.; Chen, C.; Song, W.; Zhao, J. Ligand directed debromination of tetrabromodiphenyl ether mediated by nickel under visible irradiation. *Environ. Sci. Nano* **2019**, *6*, 1585–1593. [CrossRef]

51. Huang, K.; Liu, H.; He, J.; He, Y.; Tao, X.; Yin, H.; Dang, Z.; Lu, G. Application of Ag/TiO_2 in photocatalytic degradation of 2,2′,4,4′-tetrabromodiphenyl ether in simulated washing waste containing Triton X-100. *J. Environ. Chem. Eng.* **2021**, *9*, 105077. [CrossRef]

52. Careghini, A.; Mastorgio, A.F.; Saponaro, S.; Sezenna, E. Bisphenol A, nonylphenols, benzophenones, and benzotriazoles in soils, groundwater, surface water, sediments, and food: A review. *Environ. Sci. Pollut. Res.* **2015**, *22*, 5711–5741. [CrossRef]

53. Benjamin, S.; Masai, E.; Kamimura, N.; Takahashi, K.; Anderson, R.C.; Faisal, P.A. Phthalates impact human health: Epidemiological evidences and plausible mechanism of action. *J. Hazard. Mater.* **2017**, *340*, 360–383. [CrossRef] [PubMed]

54. Swan, S.H.; Main, K.M.; Liu, F.; Stewart, S.L.; Kruse, R.L.; Calafat, A.M.; Mao, C.S.; Redmon, J.B.; Ternand, C.L.; Sullivan, S.; et al. Decrease in anogenital dis- tance among male infants with prenatal phthalate exposure. *Environ. Health Perspect.* **2005**, *113*, 1056–1061. [CrossRef]

55. Kaur, M.; Verma, A.; Setia, H.; Toor, A.P. Comparative Study on the Photocatalytic Degradation of Paraquat Using Tungsten-Doped TiO_2 Under UV and Sunlight. In *Sustainable Engineering*; Agnihotri, A., Reddy, K., Bansal, A., Eds.; Springer: Singapore, 2019; Volume 30, pp. 145–155. [CrossRef]

56. Akbari-Adergani, B.; Saghi, M.H.; Eslami, A.; Mohseni-Bandpei, A.; Rabbani, M. Removal of dibutyl phthalate from aqueous environments using a nanophotocatalytic Fe, Ag-ZnO/VIS-LED system: Modeling and optimization. *Environ. Technol.* **2018**, *39*, 1566–1576. [CrossRef]

57. Motlagh, P.Y.; Khataee, A.; Hassani, A.; Rad, T.S. ZnFe-LDH/GO nanocomposite coated on the glass support as a highly efficient catalyst for visible light photodegra- dation of an emerging pollutant. *J. Mol. Liq.* **2020**, *302*, 112532. [CrossRef]

58. Dong, W.; Zhu, Y.; Huang, H.; Jiang, L.; Zhu, H.; Li, C.; Chen, B.; Shi, Z.; Wang, G. A performance study of enhanced visible-light-driven photocatalysis and magnetical protein separation of multifunctional yolk–shell nanostructures. *J. Mater. Chem. A* **2013**, *1*, 10030–10036. [CrossRef]

59. Chang, C.F.; Man, C.Y. Titania-coated magnetic composites as photocatalysts for phthalate photodegradation. *Ind. Eng. Chem. Res.* **2011**, *50*, 11620–11627. [CrossRef]

60. Ghanbari, F.; Zirrahi, F.; Olfati, D.; Gohari, F.; Hassani, A. TiO_2 nanoparticles removal by electrocoagulation using iron electrodes: Catalytic activity of electrochemical sludge for the degradation of emerging pollutant. *J. Mol. Liq.* **2020**, *310*, 113217. [CrossRef]

61. Gu, X.; Qin, N.; Wei, G.; Hu, Y.; Zhang, Y.-N.; Zhao, G. Efficient photocatalytic removal of phthalates easily implemented over a bi-functional {001}TiO_2 surface. *Chemosphere* **2020**, *263*, 128257. [CrossRef]

62. Huang, W.-B.; Chen, C.-Y. Photocatalytic Degradation of Diethyl Phthalate (DEP) in Water Using TiO_2. *Water Air Soil Pollut.* **2010**, *207*, 349–355. [CrossRef]

63. Liao, W.; Zheng, T.; Wang, P.; Tu, S.; Pan, W. Efficient microwave-assisted photocatalytic degradation of endocrine disruptor dimethyl phthalate over composite catalyst ZrO_x/ZnO. *J. Environ. Sci.* **2010**, *22*, 1800–1806. [CrossRef]

64. Jing, Y.; Li, L.; Zhang, Q.; Lu, P.; Liu, P.; Lü, X. Photocatalytic ozonation of dimethyl phthalate with TiO_2 prepared by a hydrothermal method. *J. Hazard. Mater.* **2011**, *189*, 40–47. [CrossRef] [PubMed]

65. Kaneco, S.; Katsumata, H.; Suzuki, T.; Ohta, K. Titanium dioxide mediated photocatalytic degradation of dibutyl phthalate in aqueous solution—kinetics, mineralization and reaction mechanism. *Chem. Eng. J.* **2006**, *125*, 59–66. [CrossRef]

66. Liu, Y.; Sun, N.; Hu, J.; Li, S.; Qin, G. Photocatalytic degradation properties of α-Fe_2O_3 nanoparticles for dibutyl phthalate in aqueous solution system. *R. Soc. Open Sci.* **2018**, *5*, 172196. [CrossRef]

67. Xu, X.-R.; Li, S.-X.; Li, X.-Y.; Gu, J.-D.; Chen, F.; Li, X.-Z.; Li, H.-B. Degradation of n-butyl benzyl phthalate using TiO_2/UV. *J. Hazard. Mater.* **2009**, *164*, 527–532. [CrossRef]

68. Wang, X.-K.; Wang, C.; Jiang, W.-Q.; Guo, W.-L.; Wang, J.-G. Sonochemical synthesis and characterization of Cl-doped TiO_2 and its application in the photodegradation of phthalate ester under visible light irradiation. *Chem. Eng. J.* **2012**, *189–190*, 288–294. [CrossRef]

69. Mohamed, R.M.; Aazam, E. Synthesis and characterization of P-doped TiO_2 thin-films for photocatalytic degradation of butyl benzyl phthalate under visible-light irradiation. *Chin. J. Catal.* **2013**, *34*, 1267–1273. [CrossRef]

70. Anandan, S.; Pugazhenthiran, N.; Lana-Villarreal, T.; Lee, G.-J.; Wu, J.J. Catalytic degradation of a plasticizer, di-ethylhexyl phthalate, using $Nx–TiO_2$−x nanoparticles synthesized via co-precipitation. *Chem. Eng. J.* **2013**, *231*, 182–189. [CrossRef]

71. Eslami, A.; Akbari-Adergani, B.; Mohseni-Bandpei, A.; Rabbani, M.; Saghi, M.H. Synthesis and characterization of a coated Fe-Ag@ZnO nanorod for the purification of a polluted environmental solution under simulated sunlight irradiation. *Mater. Lett.* **2017**, *197*, 205–208. [CrossRef]

72. Zhou, W.; Yu, C.; Fan, Q.; Wei, L.; Chen, J.; Yu, J.C. Ultrasonic fabrication of N-doped TiO_2 nanocrystals with mesoporous structure and enhanced visible light photocatalytic activity. *Chin. J. Catal.* **2013**, *34*, 1250–1255. [CrossRef]

73. Singla, P.; Pandey, O.P.; Singh, K. Study of photocatalytic degradation of environmentally harmful phthalate esters using Ni-doped TiO_2 nanoparticles. *Int. J. Environ. Sci. Technol.* **2016**, *13*, 849–856. [CrossRef]

74. Ki, S.J.; Park, Y.-K.; Kim, J.-S.; Lee, W.-J.; Lee, H.; Jung, S.-C. Facile preparation of tungsten oxide doped TiO_2 photocatalysts using liquid phase plasma process for enhanced degradation of diethyl phthalate. *Chem. Eng. J.* **2018**, *377*, 120087. [CrossRef]

75. Jamil, T.S.; Abbas, H.A.; Youssief, A.M.; Mansor, E.S.; Hammad, F.F. The synthesis of nano-sized undoped, Bi doped and Bi, Cu co-doped $SrTiO_3$ using two sol–gel methods to enhance the photocatalytic performance for the degradation of dibutyl phthalate under visible light. *Comptes Rendus. Chim.* **2017**, *20*, 97–106. [CrossRef]

76. He, G.; Zhang, J.; Hu, Y.; Bai, Z.; Wei, C. Dual-template synthesis of mesoporous TiO_2 nanotubes with structure-enhanced functional photocatalytic performance. *Appl. Catal. B Environ.* **2019**, *250*, 301–312. [CrossRef]

77. Chalasani, R.; Vasudevan, S. Cyclodextrin-Functionalized Fe_3O_4@TiO_2: Reusable, Magnetic Nanoparticles for Photocatalytic Degradation of Endocrine-Disrupting Chemicals in Water Supplies. *ACS Nano* **2013**, *7*, 4093–4104. [CrossRef]

78. Shan, W.; Hu, Y.; Bai, Z.; Zheng, M.; Wei, C. In situ preparation of g-C_3N_4/bismuth-based oxide nanocomposites with enhanced photocatalytic activity. *Appl. Catal. B Environ.* **2016**, *188*, 1–12. [CrossRef]

79. Meenakshi, G.; Sivasamy, A. Nanorod ZnO/SiC nanocomposite: An efficient catalyst for the degradation of an endocrine disruptor under UV and visible light irradiations. *J. Environ. Chem. Eng.* **2018**, *6*, 3757–3769. [CrossRef]

80. Hassan, H.M.; Betiha, M.A.; El-Sharkawy, E.A.; Elshaarawy, R.F.; El-Assy, N.B.; Essawy, A.A.; Tolba, A.M.; Rabie, A.M. Highly selective epoxidation of olefins using vanadium (IV) schiff base-amine-tagged graphene oxide composite. *Colloids Surf. A Physicochem. Eng. Asp.* **2020**, *591*, 124520. [CrossRef]

81. Tang, W.; Chen, J.; Yin, Z.; Sheng, W.; Lin, F.; Xu, H.; Cao, S. Complete removal of phenolic contaminants from bismuth-modified TiO$_2$ single-crystal photocatalysts. *Chin. J. Catal.* **2021**, *42*, 347–355. [CrossRef]

82. Xu, C.; Jin, Z.; Yang, J.; Guo, F.; Wang, P.; Meng, H.; Bao, G.; Li, Z.; Chen, C.; Liu, F.; et al. A direct Z-scheme LaFeO$_3$/WO$_3$ photocatalyst for enhanced degradation of phenol under visible light irradiation. *J. Environ. Chem. Eng.* **2021**, *9*, 106337. [CrossRef]

83. Prasad, C.; Liu, Q.; Tang, H.; Yuvaraja, G.; Long, J.; Rammohan, A.; Zyryanov, G.V. An overview of graphene oxide supported semiconductors based photocatalysts: Properties, synthesis and photocatalytic applications. *J. Mol. Liq.* **2020**, *297*, 111826. [CrossRef]

84. Hurtado, L.; Amado-Piña, D.; Roa-Morales, G.; Peralta, E.; Del Campo, E.M.; Natividad, R. Comparison of AOPs Efficiencies on Phenolic Compounds Degradation. *J. Chem.* **2016**, *2016*, 1–8. [CrossRef]

85. Paschoalino, F.C.S.; Paschoalino, M.P.; Jordão, E.; Jardim, W.D.F. Evaluation of TiO$_2$, ZnO, CuO and Ga$_2$O$_3$ on the Photocatalytic Degradation of Phenol Using an Annular-Flow Photocatalytic Reactor. *Open J. Phys. Chem.* **2012**, *2*, 135–140. [CrossRef]

86. Shet, A.; Vidya, S.K. Solar light mediated photocatalytic degradation of phenol using Ag core—TiO$_2$ shell (Ag@TiO$_2$) nanoparticles in batch and fluidized bed reactor. *Sol. Energy* **2016**, *127*, 67–78. [CrossRef]

87. Rueda-Marquez, J.J.; Levchuk, I.; FernándezIbañez, P.; Sillanpää, M. A critical review on application of photocatalysis for toxicity reduction of real wastewaters. *J. Clean. Prod.* **2020**, *258*, 120694. [CrossRef]

88. Chowdhury, P.; Nag, S.; Ray, A.K. Degradation of Phenolic Compounds Through UV and Visible- Light-Driven Photocatalysis: Technical and Economic Aspects. In *Phenolic Compounds—Natural Sources, Importance and Applications*; IntechOpen: London, UK, 2017. [CrossRef]

89. Malefane, M.E. Co$_3$O$_4$/Bi$_4$O5I$_2$/Bi$_5$O$_7$I C-Scheme Heterojunction for Degradation of Organic Pollutants by Light-Emitting Diode Irradiation. *ACS Omega* **2020**, *5*, 26829–26844. [CrossRef]

90. Chowdhury, P.; Gomaa, H.; Ray, A.K. Sacrificial hydrogen generation from aqueous triethanolamine with Eosin Y-sensitized Pt/TiO$_2$ photocatalyst in UV, visible and solar light irradiation. *Chemosphere* **2015**, *121*, 54–61. [CrossRef]

91. Chowdhury, P.; Moreira, J.; Gomaa, H.; Ray, A.K. Visible-Solar-Light-Driven Photocatalytic Degradation of Phenol with Dye-Sensitized TiO$_2$: Parametric and Kinetic Study. *Ind. Eng. Chem. Res.* **2012**, *51*, 4523–4532. [CrossRef]

92. Qin, G.; Wu, Q.; Sun, Z.; Wang, Y.; Luo, J.; Xue, S. Enhanced photoelectrocatalytic degradation of phenols with biofunctionalizedd dye-sensitized TiO$_2$ film. *J. Hazard. Mater.* **2012**, *199*, 226–232. [CrossRef]

93. Rahmani, A.; Rahimzadeh, H.; Beirami, S. Photo-Degradation of Phenol Using TiO$_2$/CMK-3 Photo-Catalyst Under Medium Pressure UV Lamp. *Avicenna J. Environ. Health Eng.* **2018**, *5*, 35–41. [CrossRef]

94. Mohamed, A.; Yousef, S.; Nasser, W.S.; Osman, T.A.; Knebel, A.; Sánchez, E.P.V.; Hashem, T. Rapid photocatalytic degradation of phenol from water using composite nanofbers under UV. *Environ. Sci. Eur.* **2020**, *32*, 160. [CrossRef]

95. Górska, P.; Zaleska-Medynska, A.; Jan, H. Photodegradation of phenol by UV/TiO$_2$ and Vis/N,C-TiO$_2$ processes: Comparative mechanistic and kinetic studies. *Sep. Purif. Technol.* **2009**, *68*, 90–96. [CrossRef]

96. Liu, T.; Tan, G.; Zhao, C.; Xu, C.; Su, Y.; Wang, Y.; Ren, H.; Xia, A.; Shao, D.; Yan, S. Enhanced photocatalytic mechanism of the Nd-Er co-doped tetragonal BiVO$_4$ photocatalysts. *Appl. Catal. B Environ.* **2017**, *213*, 87–96. [CrossRef]

97. Sin, J.-C.; Lam, S.-M.; Zeng, H.; Lin, H.; Li, H.; Tham, K.-O.; Mohamed, A.R.; Lim, J.-W.; Qing, Z. Magnetic NiFe$_2$O4 nanoparticles decorated on N-doped BiOBr nanosheets for expeditious visible light photocatalytic phenol degradation and hexavalent chromium reduction via a Z-scheme heterojunction mechanism. *Appl. Surf. Sci.* **2021**, *559*, 149966. [CrossRef]

98. Zhang, Y.; Li, G.; Yang, X.; Yang, H.; Lu, Z.; Chen, R. Monoclinic BiVO$_4$ micro-/nanostructures: Microwave and ultrasonic wave combined synthesis and their visible-light photocatalytic activities. *J. Alloy. Compd.* **2013**, *551*, 544–550. [CrossRef]

99. Wang, X.; Zhou, J.; Zhao, S.; Chen, X.; Yu, Y. Synergistic effect of adsorption and visible-light photocatalysis for organic pollutant removal over BiVO$_4$/carbon sphere nanocomposites. *Appl. Surf. Sci.* **2018**, *453*, 394–404. [CrossRef]

100. Li, H.; Chen, Y.; Zhou, W.; Gao, H.; Tian, G. Tuning in BiVO$_4$/Bi$_4$V$_2$O$_{10}$ porous heterophase nanospheres for synergistic photocatalytic degradation of organic pollutants. *Appl. Surf. Sci.* **2019**, *470*, 631–638. [CrossRef]

101. Deng, Y.; Xiao, Y.; Zhou, Y.; Zeng, T.; Xing, M.; Zhang, J. A structural engineering-inspired CdS based composite for photocatalytic remediation of organic pollutant and hexavalent chromium. *Catal. Today* **2019**, *335*, 101–109. [CrossRef]

102. Mbiri, A.; Taffa, D.H.; Gatebe, E.; Wark, M. Zirconium doped mesoporous TiO$_2$ multilayer thin films: Influence of the zirconium content on the photodegradation of organic pollutants. *Catal. Today* **2019**, *328*, 71–78. [CrossRef]

103. Li, K.; Zhong, Y.; Luo, S.; Deng, W. Fabrication of powder and modular H$_3$PW$_{12}$O$_{40}$/Ag$_3$PO$_4$ composites: Novel visible-light photocatalysts for ultra-fast degradation of organic pollutants in water. *Appl. Catal. B Environ.* **2020**, *278*, 119313. [CrossRef]

104. Yu, X.; Wang, L.; Feng, L.-j.; Li, C.-h. Preparation of Au/BiOBr/Graphene composite and its photocatalytic performancein phenol degradation under visible light. *J. Fuel Chem. Technol.* **2016**, *44*, 937–942. [CrossRef]

105. Pradhan, G.K.; Padhi, D.K.; Parida, K.M. Fabrication of α-Fe$_2$O$_3$ nanorod/RGO composite: A novel hybrid photocatalyst for phenol degradation. *ACS Appl. Mater. Interfaces* **2013**, *5*, 9101–9110. [CrossRef] [PubMed]

106. Liu, H.; Su, Y.; Chen, Z.; Jin, Z.; Wang, Y. Bi7O9I3/reduced grapheme oxide composite as an efficient visible-light-driven photocatalyst for degradation of organic contaminants. *J. Mol. Catal. A Chem.* **2014**, *391*, 175–182. [CrossRef]

107. Singh, P.; Raizada, P.; Sudhaik, A.; Shandilya, P.; Thakur, P.; Agarwal, S.; Gupta, V.K. Enhanced photocatalytic activity and stability of AgBr/BiOBr/graphene heterojunction for phenol degradation under visible light. *J. Saudi Chem. Soc.* **2019**, *23*, 586–599. [CrossRef]

108. Abdullah, N.S.A.; So'aib, S.; Krishnan, J. Effect of calcination temperature on ZnO/TiO$_2$ composite in photocatalytic treatment of phenol under visible light. *Malays. J. Anal. Sci.* **2017**, *21*, 173–181.

109. Peng, W.-C.; Wang, X.; Li, X.-Y. The synergetic effect of MoS$_2$ and graphene on Ag$_3$PO$_4$ for its ultra-enhanced photocatalytic activity in phenol degradation under visible light. *Nanoscale* **2014**, *6*, 8311–8317. [CrossRef]

110. Hayati, F.; Isari, A.A.; Fattahi, M.; Anvaripour, B.; Jorfibc, S. Photocatalytic decontamination of phenol and petrochemical wastewater through ZnO/TiO$_2$ decorated on reduced graphene oxide nanocomposite: Influential operating factors, mechanism, and electrical energy consumption. *RSC Adv.* **2018**, *8*, 40035–40053. [CrossRef]

111. Teixeira, I.; Quiroz, J.; Homsi, M.; Camargo, P. An Overview of the Photocatalytic H$_2$ Evolution by Semiconductor-Based Materials for Nonspecialists. *J. Braz. Chem. Soc.* **2020**, *31*, 211–229. [CrossRef]

112. Bobirică, C.; Bobirică, L.; Râpă, M.; Matei, E.; Predescu, A.M.; Orbeci, C. Photocatalytic Degradation of Ampicillin Using PLA/TiO$_2$ Hybrid Nanofibers Coated on Different Types of Fiberglass. *Water* **2020**, *12*, 176. [CrossRef]

113. Li, M.; Li, G.; Jiang, J.; Zhang, Z.; Dai, X.; Mai, K. Ultraviolet resistance and antimicrobial properties of ZnO in the polypropylene materials: A review. *J. Mater. Sci. Technol.* **2015**, *31*, 331–339. [CrossRef]

114. Saidu, U. Synthesis and Characterization of BiVO$_4$ nanoparticles and its Photocatalytic Activity on Levofloxacin Antibiotics. *ChemSearch J.* **2019**, *10*, 104–111.

115. Yang, X.; Chen, Z.; Zhao, W.; Liu, C.; Qian, X.; Zhang, M.; Wei, G.; Khan, E.; Ng, Y.H.; Ok, Y.S. Recent advances in photodegradation of antibiotic residues in water. *Chem. Eng. J.* **2021**, *405*, 126806. [CrossRef] [PubMed]

116. Lin, H.H.-H.; Lin, A.Y.-C. Photocatalytic oxidation of 5-fluorouracil and cyclophosphamide via UV/TiO$_2$ in an aqueous environment. *Water Res.* **2014**, *48*, 559–568. [CrossRef]

117. Olusegun, S.J.; Larrea, G.; Osial, M.; Jackowska, K.; Krysinski, P. Photocatalytic Degradation of Antibiotics by Superparamagnetic Iron Oxide Nanoparticles. Tetracycline Case. *Catalysts* **2021**, *11*, 1243. [CrossRef]

118. Dong, S.; Cui, L.; Zhang, W.; Xia, L.; Zhou, S.; Russell, C.; Fan, M.; Feng, J.; Sun, J. Double-shelled ZnSnO$_3$ hollow cubes for efficient photocatalytic degradation of antibiotic wastewater. *Chem. Eng. J.* **2020**, *384*, 123279. [CrossRef]

119. Wang, H.; Ye, Z.; Liu, C.; Li, J.; Zhou, M.; Guan, Q.; Lv, P.; Huo, P.; Yan, Y. Visible light driven Ag/Ag$_3$PO$_4$/AC photocatalyst with highly enhanced photodegradation of tetracycline antibiotics. *Appl. Surf. Sci.* **2015**, *353*, 391–399. [CrossRef]

120. Guo, F.; Li, M.; Ren, H.; Huang, X.; Shu, K.; Shi, W.; Lu, C. Facile bottom-up preparation of Cl-doped porous g-C$_3$N$_4$ nanosheets for enhanced photocatalytic degradation of tetracycline under visible light. *Sep. Purif. Technol.* **2019**, *228*, 115770. [CrossRef]

121. Zhou, C.; Lai, C.; Xu, P.; Zeng, G.; Huang, D.; Zhang, C.; Cheng, M.; Hu, L.; Wan, J.; Liu, Y.; et al. In Situ Grown AgI/Bi$_{12}$O$_{17}$Cl$_2$ Heterojunction Photocatalysts for Visible Light Degradation of Sulfamethazine: Efficiency, Pathway, and Mechanism. *ACS Sustain. Chem. Eng.* **2018**, *6*, 4174–4184. [CrossRef]

122. Xiao, T.; Tanga, Z.; Yang, Y.; Tang, L.; Zhou, Y.; Zou, Z. In situ construction of hierarchical WO$_3$/g-C$_3$N$_4$ composite hollow microspheres as a Z-scheme photocatalyst for the degradation of antibiotics. *ACS Sustain. Chem. Eng.* **2018**, *220*, 417–428. [CrossRef]

123. Kumar, A.; Kumar, A.; Sharma, G.; Al-Muhtaseb, A.H.; Naushad, M.; Ghfar, A.A.; Stadler, F.J. Quaternary magnetic BiOCl/g-C$_3$N$_4$/Cu$_2$O/Fe$_3$O$_4$ nano-junction for visible light and solar powered degradation of sulfamethoxazole from aqueous environment. *Chem. Eng. J.* **2018**, *334*, 462–478. [CrossRef]

124. Kumar, A.; Khan, M.; He, J.; Lo, I.M. Visible–light–driven magnetically recyclable terephthalic acid functionalized g−C$_3$N$_4$/TiO$_2$ heterojunction nanophotocatalyst for enhanced degradation of PPCPs. *Appl. Catal. B Environ.* **2020**, *270*, 118898. [CrossRef]

125. Al Balushi, B.S.; Al Marzouqi, F.; Al Wahaibi, B.; Kuvarega, A.T.; Al Kindy, S.M.Z.; Kim, Y.; Selvaraj, R. Hydrothermal synthesis of CdS sub-microspheres for photocatalytic degradation of pharmaceuticals. *Appl. Surf. Sci.* **2018**, *457*, 559–565. [CrossRef]

126. Alberti, S.; Locardi, F.; Sturini, F.; Speltini, A.; Maraschi, F.; Costa, G.A.; Ferretti, M.; Caratto, V. Photocatalysis in Darkness: Optimization of Sol-Gel Synthesis of NP-TiO$_2$ Supported on a Persistent Luminescence Material and its Application for the Removal of Ofloxacin from Water. *J. Nanomed. Nanotechnol.* **2018**, *9*, 1–6. [CrossRef]

127. Gao, J.; Gao, Y.; Sui, Z.; Dong, Z.; Wang, S.; Zou, D. Hydrothermal synthesis of BiOBr/FeWO$_4$ composite photocatalysts and their photocatalytic degradation of doxycycline. *J. Alloy. Compd.* **2018**, *732*, 43–51. [CrossRef]

128. Gong, Y.; Wu, Y.; Xu, Y.; Li, L.; Li, C.; Liu, X.; Niu, L. All-solid-state Z-scheme CdTe/TiO$_2$ heterostructure photocatalysts with enhanced visible-light photocatalytic degradation of antibiotic wastewater. *Chem. Eng. J.* **2018**, *350*, 257–267. [CrossRef]

129. Wang, D.; Jia, F.; Wang, H.; Chen, F.; Fang, Y.; Dong, W.; Zeng, G.; Li, X.; Yang, Q.; Yuan, X. Simultaneously efficient adsorption and photocatalytic degradation of tetracycline by Fe-based MOFs. *J. Colloid Interface Sci.* **2018**, *519*, 273–284. [CrossRef]

130. Cao, Y.; Lei, X.; Chen, Q.; Kang, C.; Li, W.; Liu, B. Enhanced photocatalytic degradation of tetracycline hydrochloride by novel porous hollow cube ZnFe$_2$O$_4$. *J. Photochem. Photobiol. A Chem.* **2018**, *364*, 794–800. [CrossRef]

131. Osotsi, M.I.; Macharia, D.K.; Zhu, B.; Wang, Z.; Shen, X.; Liu, Z.; Zhang, L.; Chen, Z. Synthesis of ZnWO$_{4-x}$ nanorods with oxygen vacancy for efficient photocatalytic degradation of tetracycline. *Prog. Nat. Sci.* **2018**, *28*, 408–415. [CrossRef]

132. Suwannaruang, T.; Hildebrand, J.P.; Taffa, D.H.; Wark, M.; Kamonsuangkasem, K.; Chirawatkul, P.; Wantala, K. Visible light-induced degradation of antibiotic ciprofloxacin over Fe–N–TiO$_2$ mesoporous photocatalyst with anatase/rutile/brookite nanocrystal mixture. *J. Photochem. Photobiol. A Chem.* **2020**, *391*, 112371. [CrossRef]

133. Kumar, J.V.; Karthik, R.; Chen, S.-M.; Chen, K.-H.; Sakthinathan, S.; Muthuraj, V.; Chiu, T.-W. Design of novel 3D flower-like neodymium molybdate: An efficient and challenging catalyst for sensing and destroying pulmonary toxicity antibiotic drug nitrofurantoin. *Chem. Eng. J.* **2018**, *346*, 11–23. [CrossRef]

134. Thongam, D.D.; Chaturvedi, H. Advances in nanomaterials for heterogeneous photocatalysis. *Nano Express* **2021**, *2*, 012005. [CrossRef]

135. Tammina, S.K.; Mandal, B.K.; Kadiyala, N.K. Photocatalytic degradation of methylene blue dye by nonconventional synthesized SnO_2 nanoparticles. *Environ. Nanotechnol. Monit. Manag.* **2018**, *10*, 339–350. [CrossRef]

136. Liua, H.; Guoa, W.; Lia, Y.; Heb, S.; Hea, C. Photocatalytic degradation of sixteen organic dyes by TiO_2/WO_3-coated magnetic nanoparticles under simulated visible light and solar light. *J. Environ. Chem. Eng.* **2018**, *6*, 59–67. [CrossRef]

137. Huang, H.; Zhang, J.; Jiang, L.; Zang, Z. Preparation of cubic Cu_2O nanoparticles wrapped by reduced graphene oxide for the efficient removal of rhodamine B. *J. Alloy. Compd.* **2017**, *718*, 112–115. [CrossRef]

138. Aggarwal, S. Photo Catalytic Degradation of Methyl Orange by Using CdS Semiconductor Nanoparticles Photo catalyst. *Int. Res. J. Eng. Technol.* **2016**, *3*, 451–455.

139. Aragaw, B.A.; Dagnaw, A. Copper/reduced graphene oxide nanocomposite for high performance photocatalytic methylene blue dye degradation. *Ethiop. J. Sci. Technol.* **2019**, *12*, 125–137. [CrossRef]

140. Raina, S.; Roy, A.; Bharadvaja, N. Degradation of dyes using biologically synthesized silver and copper nanoparticles. *Environ. Nanotechnol. Monit. Manag.* **2020**, *13*, 100278. [CrossRef]

141. Zhang, Z.; Sun, L.; Wu, Z.; Liu, Y.; Li, S. Facile hydrothermal synthesis of $CuO–Cu_2O/GO$ nanocomposites for the photocatalytic degradation of organic dye and tetracycline pollutants. *New J. Chem.* **2020**, *44*, 6420–6427. [CrossRef]

142. Bharathi, P.; Harish, S.; Archana, J.; Navaneethan, M.; Ponnusamy, S.; Muthamizhchelvan, C.; Shimomura, M.; Hayakawa, Y. Enhanced charge transfer and separation of hierarchical CuO/ZnO composites: The synergistic effect of photocatalysis for the mineralization of organic pollutant in water. *Appl. Surf. Sci.* **2019**, *484*, 884–891. [CrossRef]

143. Wei, X.-N.; Ou, C.-L.; Guan, X.-X.; Peng, Z.-K.; Zheng, X.-C. Facile assembly of CdS-reduced graphene oxide heterojunction with enhanced elimination performance for organic pollutants in wastewater. *Appl. Surf. Sci.* **2019**, *469*, 666–673. [CrossRef]

144. Adhikari, S.; Chandra, K.S.; Kim, D.-H.; Madras, G.; Sarkar, D. Understanding the morphological effects of WO_3 photocatalysts for the degradation of organic pollutants. *Adv. Powder Technol.* **2018**, *29*, 1591–1600. [CrossRef]

145. Bai, X.; Du, Y.; Hu, X.; He, Y.; He, C.; Liu, E.; Fan, J. Synergy removal of Cr(VI) and organic pollutants over RP-MoS2/rGO photocatalyst. *Appl. Catal. B Environ.* **2018**, *239*, 204–213. [CrossRef]

146. Grzechulska, J.; Morawski, A.W. Photocatalytic decomposition of azo-dye acid black 1 in water over modified titanium dioxide. *Appl. Catal. B Environ.* **2001**, *36*, 45–51. [CrossRef]

147. Gnanaprakasam, A.; Sivakumar, V.M.; Thirumarimurugan, M. Influencing Parameters in the Photocatalytic Degradation of Organic Effluent via Nanometal Oxide Catalyst: A Review. *Indian J. Mater. Sci.* **2015**, *2015*, 601827. [CrossRef]

148. Senthilvelan, S.; Chandraboss, V.L.; Karthikeyan, B.; Natanapatham, L.; Murugavelu, M. TiO_2, ZnO and nanobimetallic silica catalyzedphotodegradation of methyl green. *Mater. Sci. Semicond. Process.* **2013**, *16*, 185–192. [CrossRef]

149. Karimi, L.; Zohoori, S.; Yazdanshenas, M.E. Photocatalytic degradation of azo dyes in aqueous solutions under UV irradiation using nano-strontium titanate as the nanophotocatalyst. *J. Saudi Chem. Soc.* **2014**, *18*, 581–588. [CrossRef]

150. Neppolian, B.; Kanel, S.R.; Choi, H.C.; Shankar, M.V.; Arabindoo, B.; Murugesan, V. Photocatalytic degradation of reactive yellow 17 dye in aqueous solution in the presence of TiO_2 with cement binder. *Int. J. Photoenergy* **2003**, *5*, 45–49. [CrossRef]

151. Mai, F.D.; Lu, C.S.; Wu, C.W.; Huang, C.H.; Chen, J.Y.; Chen, C.C. Mechanisms of photocatalytic degradation of Victoria Blue R using nano-TiO_2. *Sep. Purif. Technol.* **2008**, *62*, 423–436. [CrossRef]

152. Neppolian, B.; Choi, H.C.; Sakthivel, S.; Arabindoo, B.; Murugesan, V. Solar/UV-induced photocatalytic degradation of three commercial textile dyes. *J. Hazard. Mater.* **2002**, *89*, 303–317. [CrossRef]

153. Pouretedal, H.R.; Norozi, A.; Keshavarz, M.H.; Semnani, A. Nanoparticles of zinc sulfide doped with manganese, nickel and copper as nanophotocatalyst in the degradation of organic dyes. *J. Hazard. Mater.* **2009**, *162*, 674–681. [CrossRef] [PubMed]

154. Mathialagan, A.; Manavalan, M.; Venkatachalam, K.; Mohammad, F.; Oh, W.C.; Sagadevan, S. ; Sagadevan, S. Fabrication and physicochemical characterization of g-C3N4/ZnO composite with enhanced photocatalytic activity under visible light. *Opt. Mater.* **2020**, *100*, 109643. [CrossRef]

155. Qutub, N.; Singh, P.; Sabir, S.; Sagadevan, S.; Oh, W. Enhanced photocatalytic degradation of Acid Blue dye using CdS/TiO_2 nanocomposite. *Sci. Rep.* **2022**, *12*, 5759. [CrossRef] [PubMed]

156. Muthukumaran, M.; Prasath, P.V.; Kulandaivelu, R.; Sagadevan, S.; Mohammad, F.; Oh, W.C. Fabrication of nitrogen-rich graphitic carbon nitride/Cu_2O (gC3N4@ Cu_2O) composite and its enhanced photocatalytic activity for organic pollutants degradation. *J. Mater. Sci. Mater. Electron.* **2020**, *31*, 2257–2268. [CrossRef]

157. Priya, R.; Stanly, S.; Dhanalekshmi, S.B.; Mohammad, F.; Al-Lohedan, H.A.; Oh, W.C.; Sagadevan, S. Comparative studies of crystal violet dye removal between semiconductor nanoparticles and natural adsorbents. *Optik* **2020**, *206*, 164281. [CrossRef]

158. Sagadevan, S.; Lett, J.A.; Weldegebrieal, G.K.; Garg, S.; Oh, W.-C.; Hamizi, N.A.; Johan, M.R. Enhanced Photocatalytic Activity of rGO-CuO Nanocomposites for the Degradation of Organic Pollutants. *Catalysts* **2021**, *11*, 1008. [CrossRef]

159. Priya, R.; Stanly, S.; Kavitharani, T.; Mohammad, F.; Sagadevan, S. Highly effective photocatalytic degradation of methylene blue using PrO2-MgO nanocomposites under UV light. *Optik* **2020**, *206*, 164318.

160. Muthukumaran, M.; Gnanamoorthy, G.; Prasath, P.V.; Abinaya, M.; Dhinagaran, G.; Sagadevan, S.; Mohammad, F.; Oh, W.C.; Venkatachalam, K. Enhanced photocatalytic activity of Cuprous Oxide nanoparticles for malachite green degradation under the visible light radiation. *Mater. Res. Express* **2020**, *7*, 015038. [CrossRef]

161. Li, G.; Lv, L.; Fan, H.; Ma, J.; Li, Y.; Wan, Y.; Zhao, X. Effect of the agglomeration of TiO_2 nanoparticles on their photocatalytic performance in the aqueous phase. *J. Colloid Interface Sci.* **2010**, *348*, 342–347. [CrossRef]

162. Yousefi, A.; Allahverdi, A.; Hejazi, P. Effective dispersion of nano-TiO_2 powder for enhancement of photocatalytic properties in cement mixes. *Constr. Build. Mater.* **2013**, *41*, 224–230. [CrossRef]

163. Pradeev Raj, K.; Sadaiyandi, K.; Kennedy, A.; Sagadevan, S. Photocatalytic and antibacterial studies of indium-doped ZnO nanoparticles synthesized by co-precipitation technique. *J. Mater. Sci. Mater. Electron.* **2017**, *28*, 19025–19037. [CrossRef]

164. Shie, J.-L.; Lee, C.-H.; Chiou, C.-S.; Chang, C.-T.; Chang, C.-C.; Chang, C.-Y. Photodegradation kinetics of formaldehyde using light sources of UVA, UVC and UVLED in the presence of composed silver titanium oxide photocatalyst. *J. Hazard. Mater.* **2008**, *155*, 164–172. [CrossRef] [PubMed]

165. Sobana, N.; Selvam, K.; Swaminathan, M. Optimization of photocatalytic degradation conditions of Direct Red 23 using nano-Ag doped TiO_2. *Sep. Purif. Technol.* **2008**, *62*, 648–653. [CrossRef]

166. Huang, S.; Chen, C.; Tsai, H.; Shaya, J.; Lu, C. Photocatalytic degradation of thiobencarb by a visible light-driven MoS_2 photocatalyst. *Sep. Purif. Technol.* **2018**, *197*, 147–155. [CrossRef]

167. Chen, C.; Liu, J.; Liu, P.; Yu, B. Investigation of Photocatalytic Degradation of Methyl Orange by Using Nano-Sized ZnO Catalysts. *Adv. Chem. Eng. Sci.* **2011**, *1*, 9–14. [CrossRef]

168. Schneider, J.; Matsuoka, M.; Takeuchi, M.; Zhang, J.; Horiuchi, Y.; Anpo, M.; Bahnemann, D.W. Understanding TiO_2 Photocatalysis: Mechanisms and Materials. *Chem. Rev.* **2014**, *114*, 9919–9986. [CrossRef]

169. Yu, T.; Tan, X.; Zhao, L.; Yin, Y.; Chen, P.; Wei, J. Characterization, activity and kinetics of a visible light driven photocatalyst: Cerium and nitrogen co-doped TiO2 nanoparticles. *Chem. Eng. J.* **2010**, *157*, 86–92. [CrossRef]

170. Margarita Skiba, V. Vorobyova Synthesis of Ag/TiO_2 nanocomposite via plasma liquid interactions and degradation methylene blue. *Appl. Nanosci.* **2020**, *10*, 4717–4723. [CrossRef]

171. Kasinathan, K.; Kennedy, J.; Elayaperumal, M.; Henini, M.; Malik, M. Photodegradation of organic pollutants RhB dye using UV simulated sunlight on ceria based TiO_2 nanomaterials for antibacterial applications. *Sci. Rep.* **2016**, *6*, 38064. [CrossRef] [PubMed]

172. Ng, K.H.; Lee, C.H.; Khan, M.R.; Cheng, C.K. Photocatalytic degradation of recalcitrant POME waste by using silver doped titania: Photokinetics and scavenging studies. *Chem. Eng. J.* **2016**, *286*, 282–290. [CrossRef]

173. Zielińska-Jurek, A.; Kowalska, E.; Sobczak, J.; Łącka, I.; Gazda, M.; Ohtani, B.; Hupka, J.; Zaleska, A. Silver-doped TiO_2 prepared by microemulsion method: Surface properties, bio- and photoactivity. *Sep. Purif. Technol.* **2010**, *72*, 309–318. [CrossRef]

174. Asiltürk, M.; Sayılkan, F.; Arpaç, E. Effect of Fe^{3+} ion doping to TiO_2 on the photocatalytic degradation of Malachite Green dye under UV and vis-irradiation. *J. Photochem. Photobiol. A* **2009**, *203*, 64–71. [CrossRef]

175. Crişan, M.; Mardare, D.; Ianculescu, A.; Drăgan, N.; Niţoi, I.; Crişan, D.; Voicescu, M.; Todan, L.; Oancea, P.; Adomniţei, C.; et al. Iron doped TiO_2 films and their photoactivity in nitrobenzene removal from water. *Appl. Surf. Sci.* **2018**, *455*, 201–215. [CrossRef]

176. Krishnakumar, V.; Boobas, S.; Jayaprakash, J.; Rajaboopathi, M.; Han, B.; Louhi-Kultanen, M. Effect of Cu doping on TiO_2 nanoparticles and its photocatalytic activity under visible light. *J. Mater. Sci. Mater. Electron.* **2016**, *27*, 7438–7447. [CrossRef]

177. Chiang, L.F.; Doong, R. Cu-TiO_2 nanorods with enhanced ultraviolet- and visible-light photoactivity for bisphenol A degradation. *J. Hazard. Mater.* **2014**, *277*, 84–92. [CrossRef] [PubMed]

178. Nakhate, G.G.; Nikam, V.S.; Kanade, K.G.; Arbuj, S.; Kale, B.; Baeg, J.O. Hydrothermally derived nanosized Ni-doped TiO_2: A visible light driven photocatalyst for methylene blue degradation. *Mater. Chem. Phys.* **2010**, *124*, 976–981. [CrossRef]

179. Jiang, P.; Xiang, W.; Kuang, J.; Liu, W.; Cao, W. Effect of cobalt doping on the electronic, optical and photocatalytic properties of TiO_2. *Solid State Sci.* **2015**, *46*, 27–32. [CrossRef]

180. Natarajan, T.S.; Natarajan, K.; Bajaj, H.C.; Tayade, R.J. Enhanced photocatalytic activity of bismuth-doped TiO_2 nanotubes under direct sunlight irradiation for degradation of Rhodamine B dye. *J. Nanoparticle Res.* **2013**, *15*, 1–18. [CrossRef]

181. Abdelhaleem, A.; Chu, W. Photodegradation of 4-chlorophenoxyacetic acid under visible LED activated N-doped TiO_2 and the mechanism of stepwise rate increment of the reused catalyst. *J. Hazard. Mater.* **2017**, *338*, 491–501. [CrossRef]

182. Boningari, T.; Inturi, S.N.R.; Suidan, M.; Smirniotis, P.G. Novel continuous single-step synthesis of nitrogen-modified TiO_2 by flame spray pyrolysis for photocatalytic degradation of phenol in visible light. *J. Mater. Sci. Technol.* **2018**, *34*, 1494–1502. [CrossRef]

183. Grabowska-Musiał, E.; Zaleska-Medynska, A.; Sobczak, J.; Gazda, M.; Hupka, J. Boron-doped TiO_2: Characteristics and photoactivity under visible light. *Procedia Chem.* **2009**, *1*, 1553–1559. [CrossRef]

184. Yu, C.; Fan, Q.; Xie, Y.; Chen, J.; Shu, Q.; Yu, J. Sonochemical fabrication of novel square-shaped F doped TiO_2 nanocrystals with enhanced performance in photocatalytic degradation of phenol. *J. Hazard. Mater.* **2012**, *237–238*, 38–45. [CrossRef]

185. Mrowetz, M.; Selli, E. Photocatalytic degradation of formic and benzoic acids and hydrogen peroxide evolution in TiO_2 and ZnO water suspensions. *J. Photochem. Photobiol. A Chem.* **2006**, *180*, 15–22. [CrossRef]

186. Wang, C.; Li, J.; Mele, G.; Yang, G.-M.; Zhang, F.-X.; Palmisano, L.; Vasapollo, G. Efficient degradation of 4-nitrophenol by using functionalized porphyrin-TiO_2 photocatalysts under visible irradiation. *Appl. Catal. B Environ.* **2007**, *76*, 218–226. [CrossRef]

187. Xiao, Q.; Zhang, J.; Xiao, C.; Si, Z.; Tan, X. Solar photocatalytic degradation of methylene blue in carbon-doped TiO_2 nanoparticles suspension. *Sol. Energy* **2008**, *82*, 706–713. [CrossRef]

188. Abbasi, S.; Hasanpour, M. The effect of pH on the photocatalytic degradation of methyl orange using decorated ZnO nanoparticles with SnO_2 nanoparticles. *J. Mater. Sci. Mater. Electron.* **2016**, *28*, 1307–1314. [CrossRef]

189. Gusain, R.; Gupta, K.; Joshi, P.; Khatri, O.P. Adsorptive removal and photocatalytic degradation of organic pollutants using metal oxides and their composites: A comprehensive review. *Adv. Colloid Interface Sci.* **2019**, *272*, 102009. [CrossRef]

190. Nosaka, Y.; Nosaka, A. Understanding Hydroxyl Radical ($^\bullet$OH) Generation Processes in Photocatalysis. *ACS Energy Lett.* **2016**, *1*, 356–359. [CrossRef]

191. Wang, W.-Y.; Ku, Y. Effect of solution pH on the adsorption and photocatalytic reaction behaviors of dyes using TiO_2 and Nafion-coated TiO_2. *Colloids Surf. A Physicochem. Eng. Asp.* **2007**, *302*, 261–268. [CrossRef]

192. Etacheri, V.; Di Valentin, C.; Schneider, J.; Bahnemann, D.; Pillai, S.C. Visible-light activation of TiO_2 photocatalysts: Advances in theory and experiments. *J. Photochem. Photobiol. C Photochem. Rev.* **2015**, *25*, 1–29. [CrossRef]

193. Zargoosh, K.; Rostami, M.; Aliabadi, H.M. Eu^{2+}- and Nd^{3+}-Doped $CaAl_2O_4/WO_3$/polyester nanocomposite as a sunlight-activated photocatalyst for fast removal of dyes from industrial wastes. *J. Mater. Sci. Mater. Electron.* **2020**, *31*, 11482–11495. [CrossRef]

194. Alkaim, A.; Aljeboree, A.; Alrazaq, N.; Baqir, S.; Hussein, F.; Lilo, A. Effect of pH on Adsorption and Photocatalytic Degradation Efficiency of Different Catalysts on Removal of Methylene Blue. *Asian J. Chem.* **2014**, *26*, 8445–8448. [CrossRef]

195. Fatin, S.O.; Lim, H.N.; Tan, W.T.; Huang, N.M. Comparison of photocatalytic activity and cyclic voltammetry of zinc oxide and titanium dioxide nanoparticles toward degradation of methylene blue. *Int. J. Electrochem. Sci.* **2012**, *7*, 9074–9084.

196. Bahnemann, D. Photocatalytic detoxification of polluted waters. In *The Handbook of environmental Chemistry 2. Part L: Environmental Photochemistry*; Boule, P., Ed.; Springer: Berlin, Germany, 1999; pp. 285–351.

197. Hung, C.H.; Yuan, C. Reduction of Azo-dye via TiO_2–photocatalysis. *J. Chin. Inst. Environ. Eng.* **2000**, *10*, 209–216.

198. Chanathaworn, J.; Bunyakan, C.; Wiyaratn, W.; Chungsiriporn, J. Photocatalytic decolorization of basic dye by TiO_2 nanoparticle in photoreactor. *Songklanakarin J. Sci. Technol.* **2012**, *34*, 203–210.

199. Liu, C.C.; Hsieh, Y.H.; Lai, P.F.; Li, C.H.; Kao, C.L. Photodegradation treatment of azo dye wastewater by UV/TiO_2 process. *Dye. Pigment.* **2006**, *68*, 191–195. [CrossRef]

200. Sakthivel, S.; Neppolian, B.; Shankar, M.V.; Arabindoo, B.; Palanichamy, M.; Murugesan, V. Solar photocatalytic degradation of azo dye: Comparison of photocatalytic efficiency of ZnO and TiO_2. *Sol. Energy Mater. Sol. Cells* **2003**, *77*, 65–82. [CrossRef]

201. So, C.M.; Cheng, M.Y.; Yu, J.C.; Wong, P.K. Degradation of azo dye procion red MX-5B by photocatalytic oxidation. *Chemosphere* **2002**, *46*, 905–912. [CrossRef]

202. Rao, K.V.S.; Subrahmanyam, M.; Boule, P. Immobilized TiO_2 photocatalyst during long-term use: Decrease of its activity. *Appl Catal B* **2004**, *49*, 239–249. [CrossRef]

203. Nguyen, V.H.; Shawn, D.L.; Wu, J.C.S.; Bai, H. Artificial sunlight and ultraviolet light induced photo-epoxidation of propylene over V-Ti/MCM-41 photocatalyst. *J. Nanotechnol.* **2014**, *5*, 566–576. [CrossRef]

204. Taddesse, A.M.; Alemu, M.; Kebede, T. Enhanced photocatalytic activity of p-n-n heterojunctions ternary composite $Cu_2O/ZnO/Ag_3PO_4$ under visible light irradiation. *J. Environ. Chem. Eng.* **2020**, *8*, 104356. [CrossRef]

205. Zhang, J.Y.; Mei, J.Y.; Yi, S.S.; Guan, X.X. Constructing of Z-scheme 3D g-C_3N_4-ZnO@graphene aerogel heterojunctions for high-efficient adsorption and photodegradation of organic pollutants. *Appl. Surf. Sci.* **2019**, *492*, 808–817. [CrossRef]

206. Tayebee, R.; Esmaeili, E.; Maleki, B.; Khoshniat, A.; Chahkandi, M.; Mollania, N. Photodegradation of methylene blue and some emerging pharmaceutical micropollutants with an aqueous suspension of WZnO-NH_2@$H_3PW_{12}O_{40}$ nanocomposite. *J. Mol. Liq.* **2020**, *317*, 113928. [CrossRef]

207. Priya, R.; Stanly, S.; Anuradha, R.; Sagadevan, S. Evaluation of photocatalytic activity of copper ferrite nanoparticles. *Mater. Res. Express* **2019**, *6*, 095014. [CrossRef]